U.S.N.A. --- Trident Scholar project report; no. 324 (2004)

Complex Impedance Studies of Electrosprayed and Extruded Nafion Membranes

By

Midshipman 1/C Joshua M. Mueller, Class of 2004
United States Naval Academy
Annapolis, Maryland

_____
(signature)

Certification of Adviser Approval

Associate Professor Charles A. Edmondson
Physics Department

_____
(signature)

_____
(date)

Acceptance for the Trident Scholar Committee

Professor Joyce E. Shade
Deputy Director of Research & Scholarship

_____
(signature)

_____
(date)

USNA-1531-2

REPORT DOCUMENTATION PAGE

Form Approved
OMB No. 074-0188

1. AGENCY USE ONLY (Leave blank)	2. REPORT DATE	3. REPORT TYPE AND DATE COVERED
	5 May 2004	

4. TITLE AND SUBTITLE
Complex impedance studies of electrosprayed and extruded nafion membranes

5. FUNDING NUMBERS

6. AUTHOR(S)
Mueller, Joshua M. (Joshua Michael), 1982-

7. PERFORMING ORGANIZATION NAME(S) AND ADDRESS(ES)		8. PERFORMING ORGANIZATION REPORT NUMBER

9. SPONSORING/MONITORING AGENCY NAME(S) AND ADDRESS(ES)		10. SPONSORING/MONITORING AGENCY REPORT NUMBER
US Naval Academy Annapolis, MD 21402		Trident Scholar project report no. 324 (2004)

11. SUPPLEMENTARY NOTES

12a. DISTRIBUTION/AVAILABILITY STATEMENT	12b. DISTRIBUTION CODE
This document has been approved for public release; its distribution is UNLIMITED.	

13. ABSTRACT: Fuel cells and other alternate forms of power and power generation have recently become a focal point of increased technological interest. One promising type of fuel cell is based on the Proton Exchange Membrane (PEM). Nafion 117 is one of the current benchmark membranes being used in these fuel cells. The aim of this study was to conduct fundamental scientific research into the proton transport properties of Nafion polymer membranes produced using various deposition techniques. The main focus was a comparison between electrosprayed and traditional extruded films. In addition, a study of the orientation effects in extruded Nafion membranes was conducted. Although the deposition technique of electrospraying has been used for nearly a century, it has only recently been applied to PEM fuel cell membranes. In this application, the method of deposition is designed to reduce the fabrication costs of fuel cells. Tests including measurements of conductivity, swelling effects, and activation volumes in relation to changing environmental pressures and relative humidities were performed on samples formed by the two deposition techniques. Conductivity is a measurement of the ease of passing charge carriers, while activation volume is a parameter that is helpful in determining proton transport mechanisms. Activation volumes in certain regimes are indicative of either polymer side chain deformation, Grotthuss transport, or vehicular transport of protons. These studies found a close correlation in the results comparing bulk conductivities for the two deposition techniques. The activation volumes found for the electrosprayed and extruded membranes followed the same response to changing water contents. Electrosprayed Nafion was found to have greatly increased water absorption at high relative humidities in comparison to the raditional extruded samples; however, the bulk conductivities remained comparable. The orientation studies in low water content extruded Nafion 117 showed an approximate difference of two orders of magnitude in conductivity when comparing cross-plane measurements to in-plane measurements, traditionally studied for these materials. These results indicate that electrospraying is an effective and efficient means of depositing PEM fuel cell membranes, which may lead to mass production of fuel cells.

14. SUBJECT TERMS: Impedance Spectroscopy; Nafion; Electrospraying; Proton Exchange Membrane Fuel Cells	15. NUMBER OF PAGES 68
	16. PRICE CODE

17. SECURITY CLASSIFICATION OF REPORT	18. SECURITY CLASSIFICATION OF THIS PAGE	19. SECURITY CLASSIFICATION OF ABSTRACT	20. LIMITATION OF ABSTRACT

Abstract

Fuel cells and other alternate forms of power and power generation have recently become a focal point of increased technological interest. One promising type of fuel cell is based on the Proton Exchange Membrane (PEM). Nafion 117 is one of the current benchmark membranes being used in these fuel cells. The aim of this study was to conduct fundamental scientific research into the proton transport properties of Nafion polymer membranes produced using various deposition techniques. The main focus was a comparison between electrosprayed and traditional extruded films. In addition, a study of the orientation effects in extruded Nafion membranes was conducted.

Although the deposition technique of electrospraying has been used for nearly a century, it has only recently been applied to PEM fuel cell membranes. In this application, the method of deposition is designed to reduce the fabrication costs of fuel cells. Tests including measurements of conductivity, swelling effects, and activation volumes in relation to changing environmental pressures and relative humidities were performed on samples formed by the two deposition techniques. Conductivity is a measurement of the ease of passing charge carriers, while activation volume is a parameter that is helpful in determining proton transport mechanisms. Activation volumes in certain regimes are indicative of either polymer side chain deformation, Grotthuss transport, or vehicular transport of protons.

These studies found a close correlation in the results comparing bulk conductivities for the two deposition techniques. The activation volumes found for the electrosprayed and extruded membranes followed the same response to changing water contents. Electrosprayed Nafion was found to have greatly increased water absorption at high relative humidities in comparison to the traditional extruded samples; however, the bulk conductivities remained comparable. The orientation studies in low water content extruded Nafion 117 showed an approximate difference of two orders of magnitude in conductivity when comparing cross-plane measurements to in-plane measurements, traditionally studied for these materials. These results indicate that electrospraying is an effective and efficient means of depositing PEM fuel cell membranes, which may lead to mass production of fuel cells.

Keywords:

Impedance Spectroscopy

Nafion

Electrospraying

Proton Exchange Membrane Fuel Cells

Acknowledgements

I am grateful for the work of my collaborators: Professors Fontanella and Wintersgill; Dr. Greenbaum of Hunter College for his Nuclear Magnetic Resonance research; Dr. Suarez of the Naval Research Lab; finally, Dr. Wnek of Virginia Commonwealth University for providing me with the samples on which the entire project revolved.

I would also like to thank Professors Ferrante, Zak, and Andre for their help in serving as my Trident Committee Guides, as well as Dr. Shade for her help as the Trident Committee Chair.

I am also thankful for the financial aid of the Office of Naval Research and the Kinnear Fellowship. ONR provides the funding for the condensed matter research group at the Academy. The Kinnear Fellowship and support from the Academic Dean have enabled Professor Edmondson to take a year-long sabbatical devoted to research. Professor Edmondson has dedicated a considerable portion of his sabbatical towards aiding me on this project.

Thanks to my parents for their support for eighteen years at home, and now four years at the Naval Academy. Without their love and generosity I could never have made it this far.

Lastly, I'd like to extend my humblest appreciation to Professor and Mrs. Edmondson for their aid through this semester in my pursuit of graduate education.

Table of Contents

Abstract	Page 1
Acknowledgements	Page 2
Table of Contents	Page 3
List of Figures	Page 4
I Introduction	Page 6
II Background Information	Page 7
A. Fuel Cells	Page 7
B. Nafion	Page 9
C. Electrospraying	Page 11
D. Impedance Spectroscopy	Page 12
E. Conductivity and Activation Volume	Page 18
F. Dielectric Relaxation	Page 21
G. Nuclear Magnetic Resonance	Page 27
III Materials and Instruments	Page 30
IV Methods	Page 31
V Results	Page 38
A. Water Absorption and Dimensional Stability	Page 38
B. Conductivity Comparisons	Page 42
C. Dielectric Relaxation	Page 46
D. Activation Volume	Page 49
E. Nuclear Magnetic Resonance	Page 51

F. Orientation Effects on Conductivity Page 55

VI Conclusion Page 61

Appendix A: Dynamic Mechanical Analysis Page 64

VII References Page 66

List of Figures

Figure II.A.1 Simple Fuel Cell Model Page 8

Figure II.B.1 Nafion Molecular Structure Page 10

Figure II.C.1 Electrospraying Process Page 12

Figure II.D.1 Impedance Arc Page 13

Figure II.D.2 Phasor Diagram Page 14

Figure II.D.3 Simple Circuit Model Page 15

Figure II.D.4 Arc with Electrode Blocking Page 17

Figure II.D.5 Circuit Model with Electrode Blocking Page 18

Figure II.E.1 Typical Conductivity Plot for Nafion 117 Page 19

Figure II.F.1 Parallel Plate Capacitor in Free Space Page 23

Figure II.F.2 Parallel Plate Capacitor with a Dielectric Medium Page 23

Figure II.F.3 Phasor Diagram Relating Charge, Current, and Potential Page 24

Figure II.F.4 Arrhenius Plot of Gamma Peak for Electrosprayed Nafion Page 27

Figure IV.1 In-Plane Sample Page 31

Figure IV.2 Cross-Plane Sample Page 32

Figure IV.3 Sample Plot of Data Taken via a Hysteresis Loop Page 34

Figure IV.4 Hermetically Sealed Sample Page 35

Figure V.A.1 Water Content vs. Relative Humidity Page 40

Figure V.A.2 Change in Length vs. Water Content Page 41

Figure V.B.1 Conductivity vs. Water Content Page 43

Figure V.B.2 Impedance Arc with Minimal Electrode Blocking Page 44

Figure V.B.3 Impedance Arc Distorted by Electrode Blocking Regions Page 45

Figure V.C.1 Complex Dielectric Constant for Electrosprayed Nafion Page 47

Figure V.C.2 Arrhenius Plot of Gamma Peak for Electrosprayed Nafion Page 48

Figure V.D.1 Activation Volume vs. Water Content Page 49

Figure V.E.1 Diffusion Coefficients Page 51

Figure V.E.2 Spin Lattice Relaxation Times Page 52

Figure V.E.3 NMR spectra at 20º C for Electrospray and extruded Nafion Page 53

Figure V.E.4 Orientation Diffusion Coefficients for Nafion 117 Page 55

Figure V.F.1 Orientation Effects on Conductivity for Nafion 117 Page 57

Figure V.F.2 Orientation Effects for Electrosprayed Nafion and Nafion 117 Page 59

Figure V.F.3 Orientation Effects on Activation Volume for Nafion 117 Page 60

I Introduction

Fuel cell technology is an area of research and development that has recently received a great deal of focus and funding. President Bush's 2003 State of the Union Address highlighted a plan to devote $1.2 billion to the development of a car able to run on hydrogen-powered fuel cells. Similarly, the Office of Naval Research put forward its Grand Challenges for the 21st Century, in which one of the challenges was the development of "new, safe, efficient, environmentally friendly, non-petroleum based sources of power and power generation."[1] Fuel cells provide a promising possibility for this challenge. One type of fuel cell is a Proton Exchange Membrane (PEM) fuel cell, which is built around a proton conducting polymer. Years of research confirm that before any significant progress can be made, a greater understanding of the basic physical behaviors of conducting polymers is needed. The purpose of this project is to conduct fundamental scientific research into the material properties of fuel cell polymer membranes with an emphasis on conductivity-related phenomena.

This project specifically focuses on the properties of Electrosprayed Nafion. Electrospray deposition[2] is a technique being applied for the first time to polymer membranes because of its potential for mass fabrication of fuel cells. The results are compared to those of commercially extruded Nafion 117 and cast Nafion, the conventional production processes. Nafion has long been considered one of the benchmark materials for hydrogen powered fuel cell research. It is a good conductor of protons, while being gas impermeable and structurally strong. However, Nafion 117 is expensive to manufacture, and even more costly to build into the Membrane Electrode Assembly (MEA) of a fuel cell. This project does not directly focus on the development or the chemical engineering of the polymers in question. However, in the tradition

of scientific cooperation, the findings of this project have provided feedback to those in the development phase to aid in the engineering and manufacturing of the future generation of hydrogen powered fuel cell membranes. As a result of collaboration with researchers at Hunter College performing Nuclear Magnetic Resonance (NMR) studies of the same polymers, a better understanding of proton transport in these materials has been gained.

The specific aspects of the materials being studied in the project encompass both macroscopic and microscopic properties of Electrosprayed and extruded Nafion. The microscopic properties include diffusion of water as measured by NMR and dielectric resonance characteristics. The macroscopic properties include comparisons of the dimensional swelling due to water absorption, conductivity, and activation volume. The NMR research also provided a key insight into the orientation-dependent differences in proton transport observed in Nafion 117. The conductivities and activation volumes for these orientations are compared, as well as a comparison of the orientation-dependent conductivities for Electrospray Nafion.

II Background Information

This project covers a broad range of topics in the realm of physics. At times it draws on electromagnetic theory, while at others it walks the line differentiating physics and chemistry. This report contains a primer on fuel cell fundamentals, Nafion structure, electrospraying technique and impedance spectroscopy. Some results of this study have been duplicated and presented in this section to aid the discussion of the background material.

A. Fuel Cells:

Fuel cells[3] are essentially batteries designed to operate on a replenishable fuel source such as H_2 and O_2. Fuel cells produce an electric current using stored chemical energy. In a

Proton Exchange Membrane[4] (PEM) fuel cell, chemical reactions occur at the electrodes, and protons are transported via a membrane from one electrode to the other. Hydrogen powered fuel cells use a variety of energy sources ranging from hydrogen gas to hydrocarbon derivatives such as methanol or ethanol, all of which react with oxygen[5]. In addition to PEM fuel cells there are solid oxide fuel cells that have a ceramic material instead of a polymer membrane, and are designed to run at high temperatures. Solid oxide fuel cells provide increased efficiency when used at design temperatures, but require an increased initial input of energy to reach those conditions.

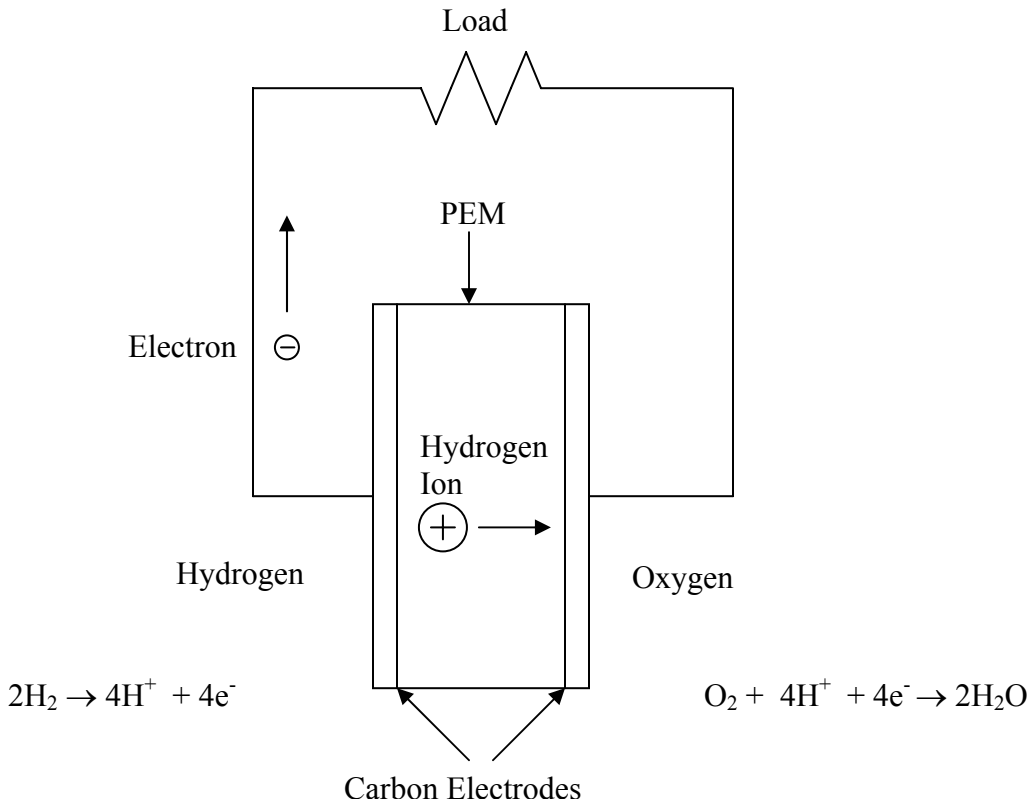

Figure II.A.1 Simple Fuel Cell Model

The basic PEM fuel cell uses a Membrane Electrode Assembly (MEA) to produce an electric current from the hydrogen and the oxygen. This is illustrated in Figure II.A.1. The H_2 comes into contact with a carbon and platinum electrode. The Pt acts as a catalyst to split the molecule into hydrogen ions and electrons. The electrons flow from this electrode to do work through a load. The ions travel through the membrane to the other side where there is another carbon and platinum electrode. At this electrode, the hydrogen ions, electrons that have moved through the load, and oxygen available from the atmosphere combine to create a water molecule. These water molecules, as well as some thermal energy, are the only waste products from a hydrogen / oxygen fuel cell.

There are several considerations that must be accounted for in the membrane. First of all, it must be of a material that allows for proton mobility, but blocks the movement of larger molecules, specifically oxygen. The fuel sources must be relatively pure. The presence of impurities such as CO can poison the chemical reactions at the electrode. Most membrane materials use water in the proton transport process. The membrane material must have good water transport properties including water molecule mobility and limited swelling due to water. If a membrane doesn't evenly disperse water, the conductance can be affected, and increased resistance in dry areas can cause hot spots that may structurally damage the fuel cell. The membrane should be strong and durable in a variety of conditions. Large-scale applications are also affected by membrane cost, although the ideal fuel cell is dependent on a myriad of other factors as well.

B. Nafion:

One of the best PEMs available is Nafion[6]. Nafion is composed of a long fluoro-carbon chain with various short side chains branching off it, as illustrated in Figure II.B.1. In Nafion

117, there is approximately one side chain for every 13 CF_2 in the polymer backbone.[7,8] In the acid form, these side chains end in a sulfonate group. Water clusters about the sulfonate and solvates the proton. The proton becomes the mobile charge carrier and the side chain is left with a negative charge. These clusters of water molecules around a sulfonate provide the means of transportation for protons through the membrane. It has been found in previous studies that as the water content of the material increases, the conductivity increases as well.[9] Thus, the water that is created by the combination of hydrogen and oxygen in the PEM actually leads to increased efficiency in the membrane (up to a point). Fuel cells must have good water transport properties to insure that the created water is evenly distributed so that hot spots of increased resistance don't develop. Also, too much water can inversely impact the chemical reactions, although most PEMs today require at least an initial wetting of the membrane to commence efficient proton conduction.

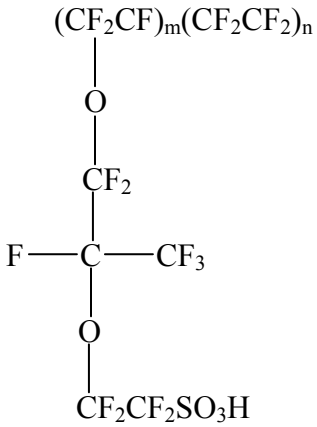

Figure II.B.1 Nafion Molecular Structure

Nafion is used in a variety of applications. It was created by the DuPont Chemical Engineering company in the mid 1970's. One significant problem with Nafion is its cost.

Researchers are now in the process of trying to find reasonable substitutes at economically useful prices. Electrospraying Nafion might offset the high polymer cost by reducing expenses associated with the fabrication of the MEAs. In this process, the Nafion is electrosprayed in sheets onto a spinning drum. If the Electrosprayed Nafion maintains the physical properties of extruded Nafion it might be a useful substitute as a PEM. Such a substitute would have the potential of creating an entire MEA, in one step, by electrospraying the membrane and electrodes, thus reducing fabrication costs.

C. Electrospraying:

In the electrospraying fabrication process, the material to be electrosprayed is taken in liquid form, and mixed with an alcohol solvent. It passes through a syringe maintained at a potential of 10 to 20 kilovolts, relative to a grounded target drum. The material accelerates toward the slowly rotating and translating drum. As the Nafion solution accelerates towards the drum, charged droplets form, due to the evaporation of the alcohol solvent, as opposed to a steady stream. The continued evaporation of the solvent also causes the droplets of Nafion solution to contract in size. The coulomb repulsion experienced by the charged polymers increases as a result of the decreasing separation between molecules due to the evaporating solvent. This repulsion leads to even smaller droplets, such that upon contact with the drum, the solution forms a membrane as the droplets are discharged. Figure II.C.1 illustrates the electrospraying process.[10]

The goal behind the development of this new fabrication technique is to be able to electrospray an electrode onto the drum, then to electrospray the PEM over that, and finally to electrospray the other electrode. Similarly to Nafion, the carbon and platinum for the electrode would have to be dissolved or suspended in an appropriate solvent. This would create the entire

MEA in one step. The process would be quicker and easier than the current technique of extruding the Nafion in order to form a membrane, and then sandwiching the membrane between the electrodes. This method of extrusion then sandwiching is a highly labor intensive method. Electrospraying may enable simpler mass production of hydrogen powered fuel cells.

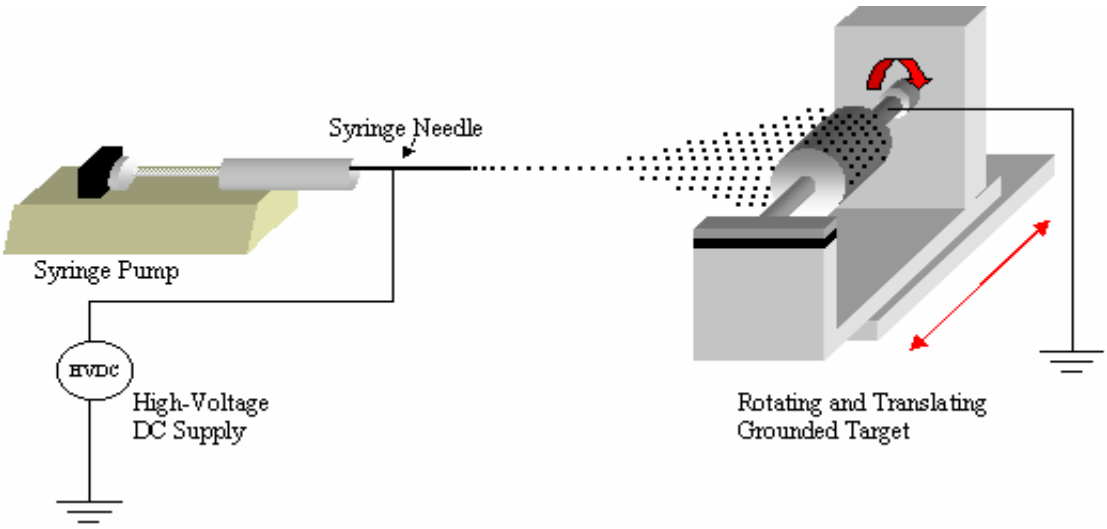

Figure II.C.1 Electrospraying Process[10]

D. Impedance Spectroscopy:

The PEM is studied with an impedance[11] bridge. The bridge applies an AC voltage at various frequencies and measures the complex impedance. The data is then analyzed as impedance arcs, with real impedance on the x-axis, and imaginary impedance on the y-axis. The impedance manifests itself as a phase difference between the current through the sample and the electric potential applied to the sample. This phase difference arises from the dielectric

properties of the materials being studied. An idealized impedance arc for a membrane sample is shown below in Figure II.D.1.

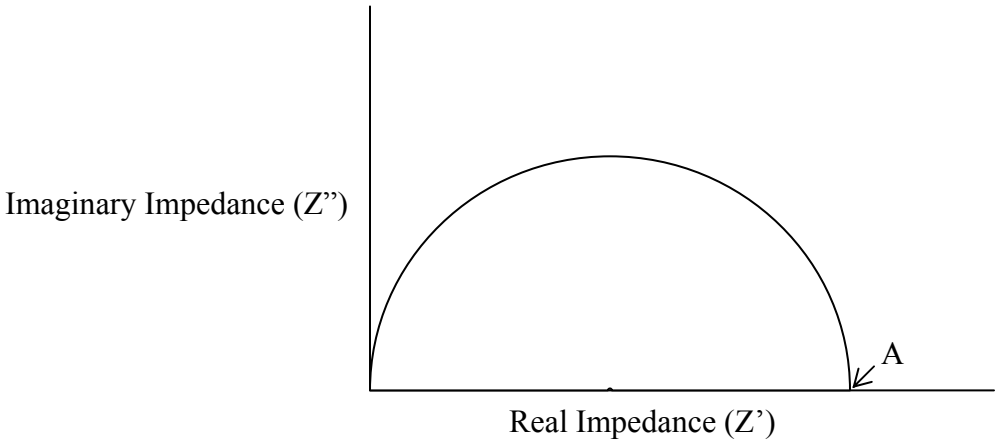

Figure II.D.1 Impedance Arc

The resistance of the sample is given by the non-zero x-intercept of the circular portion of the impedance arc as shown by point A in Figure II.D.1. The arc is a product of the electrical properties of the material. The mathematical foundations for the arc can be derived from basic electromagnetic theory.

Ohm's Law $V = IR$ (note this is for a DC element) Eq II.D.1

Ohm's Law for AC $V(\omega,t) = I(\omega,t)Z(\omega)^*$ Eq II.D.2

Where the Complex Impedance is $Z^* = Z' + iZ''$ Eq II.D.3

Where i is the imaginary constant $i = \sqrt{-1}$ and the ω dependence of the impedance is dropped for the simplicity of notation.

The phase shift between the phasors for the current and voltage is accounted for by the complex impedance.

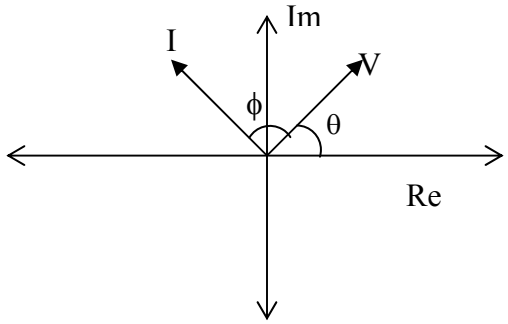

Figure II.D.2 Phasor Diagram

Mechanically this phenomenon can be visualized by imagining the electrons as small point charges. As the periodic potential is applied there is a resulting current, observed as the motion of the electrons. In the phasor diagram, Figure II.D.2, the voltage oscillates in direction, rotating about the origin at a frequency ω. The angle θ in this figure is equal to ωt and ϕ is the phase difference between the Current and Voltage Phasors. The changing real component of the magnitude can be plotted as a time dependent sinusoid, as can the imaginary component. The real component is $V_R = V_0 \cos(\omega t)$, where V_0 is the amplitude, and the imaginary is $V_I = V_0 \sin(\omega t)$. Combining these two components using Euler's, the potential becomes $V(\omega, t) = V_0 e^{i\omega t}$. The same is true of the phasor for the current.

Because materials used in a PEM fuel cell are dielectric as well as conductive in nature, they can be modeled by a circuit element of a resistor in parallel with a capacitor.

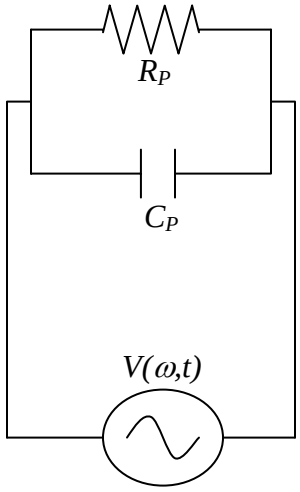

Figure II.D.3 Simple Circuit Model

In the diagram above, Figure II.D.3, R_P is the bulk resistance of the membrane, and C_P accounts for the dielectric nature of the material. The P suffix is used to denote the fact that the resistive and capacitive effects are modeled in a circuit as elements in parallel. The relationship between Z^* and R_P and C_P can be found by exploring the properties of the various currents in the circuit model.

$$I_R = \frac{V(\omega,t)}{R_P} \qquad \text{Eq II.D.4}$$

$$I_C = C_P \frac{\partial(V(\omega,t))}{\partial(t)} \qquad \text{Eq II.D.5}$$

$$I(\omega,t) = I_R + I_C = \frac{V(\omega,t)}{Z^*} \qquad \text{Eq II.D.6}$$

Assuming a voltage in Euler's form $V(\omega,t) = V_0 e^{i\omega t}$

$$\frac{1}{Z^*} = \frac{1}{R_P} + C_P(i\omega) \qquad \text{Eq II.D.7}$$

Solving for Z^*

$$Z^* = \frac{R_P}{1 + iR_P C_P \omega} \qquad \text{Eq II.D.8}$$

Z^* can be split into real and imaginary components by multiplying both the numerator and the denominator by the complex conjugate of the denominator.

$$Z^* = \frac{R_P(1 - iR_P C_P \omega)}{1 + R_P^2 C_P^2 \omega^2} = \frac{R_P}{1 + R_P^2 C_P^2 \omega^2} + i\frac{R_P^2 C_P \omega}{1 + R_P^2 C_P^2 \omega^2} = Z' + iZ'' \qquad \text{Eq II.D.9}$$

$$Z' = \frac{R_P}{1 + R_P^2 C_P^2 \omega^2} \qquad \text{Eq II.D.10}$$

$$Z'' = \frac{R_P^2 C_P \omega}{1 + R_P^2 C_P^2 \omega^2} \qquad \text{Eq II.D.11}$$

$$(Z')^2 - (Z'')^2 = \frac{R_P^2}{1 + R_P^2 C_P^2 \omega^2} \qquad \text{Eq II.D.12}$$

By completing the squares in the above equation, Eq II.D.12, one derives the equation for a circle of radius $\frac{R_P}{2}$, centered at $\frac{R_P}{2}$.

$$\left[Z' - \frac{R_P}{2}\right]^2 + \left[Z''\right]^2 = \left[\frac{R_P}{2}\right]^2 \qquad \text{Eq II.D.13}$$

From Eq II.D.13 the resulting real axis intercepts of this circle are $Z' = 0$ and $Z' = R_P$. Thus, the second intercept of the arc is the bulk resistance of the material.

In the actual experimentation, there is an additional complexity that arises from the nature of the polymers being studied. The second Z' intercept frequently is not observed in an actual complex impedance plot, and thus must be extrapolated from curve fitting techniques that use the

symmetry of the arc to find the intercept. The reason for the missing intercept is the electrode blocking effect.

Because the measurement is being performed on proton conducting membranes, and the frequency response analyzing equipment studies electron current, the resulting impedance arc has an additional complication. In the electrode blocking effect, at low frequencies, there is an electric field that counters the applied potential. Imagine the protons as positive point charges. At low frequencies, they begin to pile up at the membrane-electrode interface, because they are not mobile within the metal electrode. The protons then create an electric field in the opposite direction, greatly reducing the current. This is less of a consideration at high frequencies, in which the protons oscillate and thus change direction before too much charge builds up at the interface. As long as the impedance arc dominates the response such that over half the arc is observed, point A, the bulk resistance, can be found. The blocking effect appears on the graph, as illustrated in Figure II.D.4, as a rapid increase in the imaginary impedance.

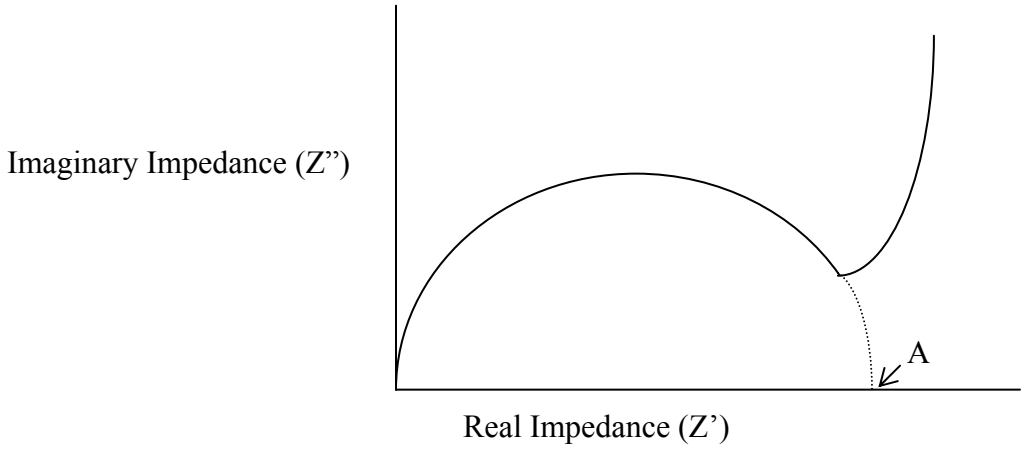

Figure II.D.4 Arc with Electrode Blocking

In order to model this new effect an additional capacitor is added in series with the original model, shown in Figure II.D.5. This capacitor acts in the same manner as a high pass filter, in which the current is driven to zero as the frequency decreases.

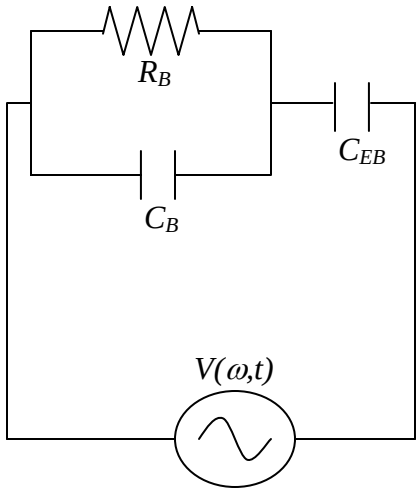

Figure II.D.5 Circuit Model with Electrode Blocking

E. Conductivity and Activation Volume:

The conductance, *G*, of the sample is found by taking the inverse of the resistance $G = \frac{1}{R}$, and is therefore dependent on the dimensions of the sample. This dependence may be removed by finding the conductivity, σ, where $\sigma = \frac{lG}{A} = \frac{l}{RA}$. A is the cross-sectional area of the sample and *l* is the length. Studying the conductivity of the sample enables the researcher to observe bulk properties that can be applied to any size and shape. Figure II.E.1 shows a typical

graph of the conductivity of Nafion 117 at various weight percent water absorbed by the membrane.

The conductivity of Nafion 117 is clearly water dependent[12]. It is actually water molecules clustering around the hydrophilic sulfonate group that liberate and transport the proton[13]. Thus, at low weight percent water the material has an exceedingly low conductivity, which corresponds to a large bulk resistance for the sample. At high water content there are two methods by which the protons are thought to move through the membrane. The first is the Grotthuss mechanism, in which the protons are exchanged from one water molecule to the next.[14] The other is a vehicular transport, in which a proton attaches to a water molecule to form a hydronium ion. This ion then moves through the membrane, thus achieving the same effect, conductance.

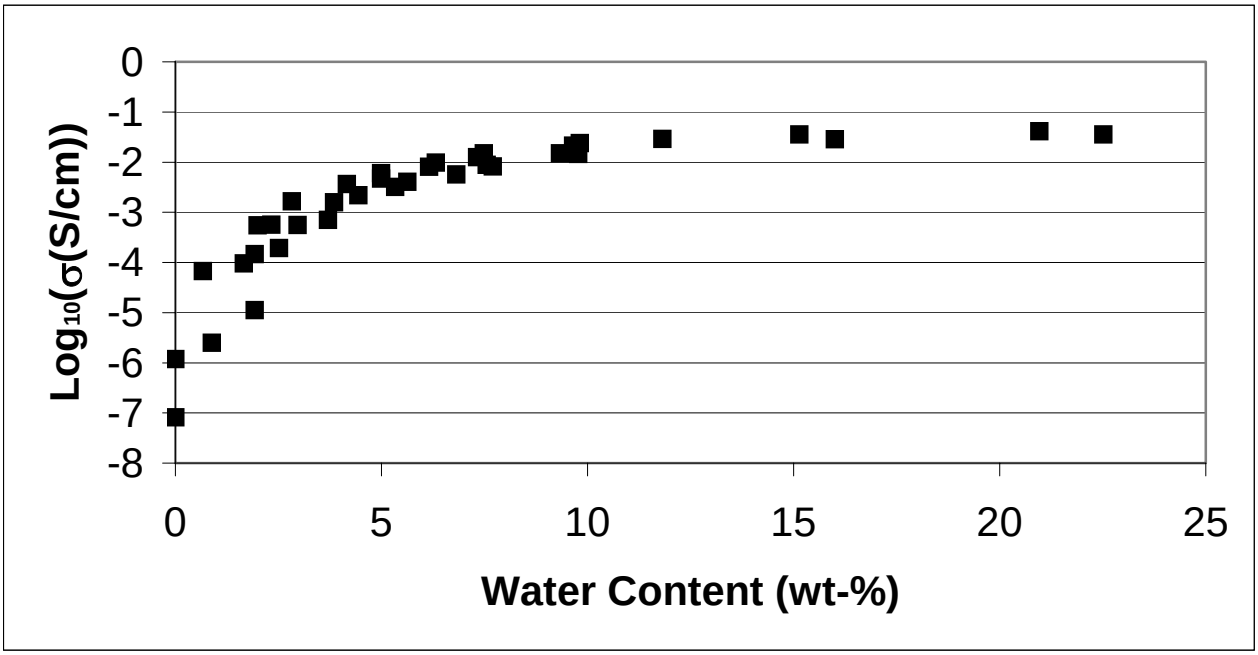

Figure II.E.1 Typical Conductivity Plot for Nafion 117

Activation volume is a thermodynamic variable that is a measure of how difficult it is to move a charge carrier through the lattice. Activation volume represents a structural deformation in the material. In this way it is a measure of how the polymer chains react during proton transport. As the hydrogen ions are pushed through the membrane, the polymer must physically move in order to respond to the motion of the proton. Activation volume, ΔV, will be used as an indication of the proton transport mechanism. The units of activation volume are cm^3/mole.

Activation volume is calculated from the pressure dependence of the logarithmic conductance at constant temperature, $\left(\frac{\partial \ln(G)}{\partial P}\right)_T$. Multiplying this expression by Boltzmann's constant and the temperature, and subtracting a correction factor based on the compressibility of the material, one has the activation volume, ΔV as shown in Eq II.E.1.

$$\Delta V = kT\left(\left(\frac{\partial \ln(G)}{\partial P}\right)_T - 0.1\right) \qquad \text{Eq II.E.1}$$

where 0.1 is the approximate compressibility factor. No data exists to fully define the compressibility factor for Nafion 117, so it was assumed to be similar to poly-(tetrafluoroethylene).[15] The same compressibility factor was also used for Electrosprayed Nafion.

The current model of activation volume applied to Nafion helps clarify the proton transport mechanism. At high water content the activation volume is very similar to that of water. This is consistent with the idea that water molecules provide the conductance path for the hydrogen ions, by either the Grotthuss mechanism or vehicular transport. Water has a negative activation volume, indicating a compression or collapsing channel for proton conduction. This is true in Grotthuss mechanism, which has a low activation volume as a result of the breaking of

large polar bonded molecules such as $H_9O_4^+$. The higher the water content, the more likely the PEM is to behave as though it were pure water. At lower water contents, the theory is that the side chains must move to allow proton transfer. The swinging of these side chains would result in larger activation volumes.

F. Dielectric Relaxation

Conductivity and activation volume are both macroscopic properties of fuel cell membranes. Dielectric relaxation is a way to study some of the microscopic properties of the material.[16] This type of study focuses on events taking place at the molecular or near molecular level of the sample. It provides information regarding the samples ability to store or dissipate energy. In this technique the sample is driven at audio frequencies and the response is analyzed in terms of a resonance phenomenon.

A powerful analogy to the effects occurring in dielectric relaxation is a damped mass on a spring. When driven at most frequencies, the mass will dissipate energy to the environment through drag and frictional forces acting on it. At certain frequencies, however, large amounts of applied energy will be stored in the system as an increase in amplitude. This is known as a resonant frequency. At resonance, the systems ability to store energy peaks in comparison to the background trends.

In dielectric relaxation, a changing electric field drives dipoles within the system in the same way that one drives a mass on a spring with a mechanical oscillation. This provides a series of responses from the material. Because of the complex interaction of molecules, there will be a lag between their polarization and the applied field. This lag is caused by energy that has been lost through dissipation into heat. The dipoles that polarize with respect to the field have not been identified for Nafion 117, although it is assumed that it is an element of the side

chain. The lost thermal energy is irretrievable, as opposed to the energy that is stored in the polarization of the molecules. Relaxation is the term used to describe the mechanism for giving up energy.

Results from a study of dielectric relaxation generally come in the form of a complex dielectric constant $\varepsilon^* = \varepsilon' - i\varepsilon''$ and a loss tangent, $\tan(\delta)$. Where:

$$\varepsilon' = \frac{C_P}{C_0} \qquad \text{Eq II.F.1}$$

C_P is the parallel capacitance of the sample and C_0 is the empty cell capacitance of the material.[17] The empty cell capacitance is defined by the dimensions of the sample such that

$$C_0 = \frac{\varepsilon_0 A}{d} \qquad \text{Eq II.F.2}$$

where ε_0 is the permittivity of free space, a physical constant of nature.

Both C_P and C_0 are defined in terms of the sample area, A, and the distance between plates, d. Thus, the real part of the dielectric constant accounts for the increased capacitance of the dielectric medium. This increased capacitance is a way to store energy, in the form of polarized dipoles, in the medium. Figure II.F.1 is a diagram of a parallel plate capacitor operating in free space. The + and – signs represent free charges on the plate, and the arrows represent the electric field lines. The empty cell capacitance, C_0, is related to the total amount of energy that can be stored in a capacitor without a dielectric, in the form of an electric field between the two plates. For a fixed potential difference, the electric field is a function of the capacitor dimensions, and does not change with the addition of a dielectric.

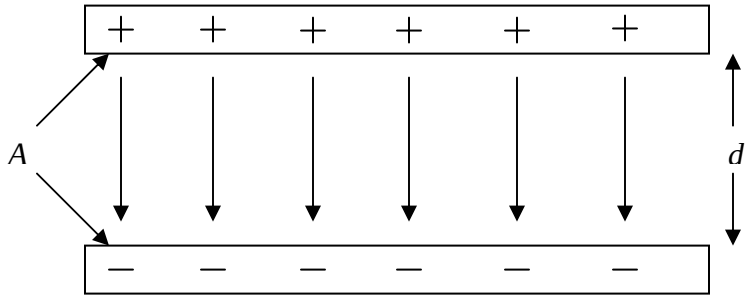

Figure II.F.1 Parallel Plate Capacitor in Free Space

If a dielectric medium is added to the capacitor, the bulk capacitance. This is because, for a fixed potential difference, more charges can be placed on the plate without increasing the electric field between the plates. This process is accounted for by the alignment of dipole molecules within the dielectric. This is shown in Figure II.F.2.

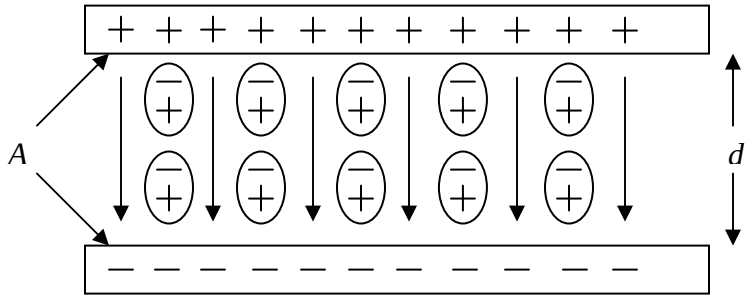

Figure II.F.2 Parallel Plate Capacitor with a Dielectric Medium

For an ideal dielectric, the additional stored charge and energy would be the end of the story. However, Nafion is a material that both polarizes and conducts. The imaginary component of

the dielectric constant is related to the energy lost through dissipation of heat in the material. It is described by:

$$\varepsilon'' = \frac{G_P}{\omega C_0} \qquad \text{Eq II.F.3}$$

where G_P is the equivalent parallel conductance of the sample. Conduction in most solids implies an interaction between the charge carriers and the solid. This interaction involves a transfer of energy, and therefore, this term accounts for energy lost as heat.

Thus, the imaginary part of the dielectric constant is a measure of the energy lost in the system, while the real component accounts for energy that has been stored within the material. Both the real and imaginary part of the dielectric constant have a role in defining the microscopic behavior of these materials when a changing electric field is applied.

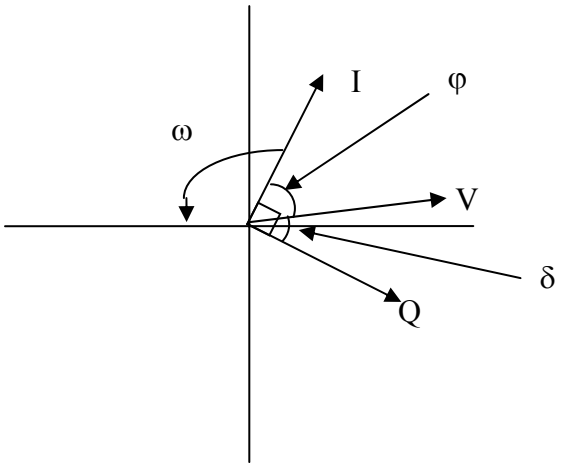

Figure II.F.3 Phasor Diagram Relating Charge, Current, and Potential

The loss tangent is both the ratio of the imaginary to real part of the dielectric constant, $\tan(\delta) = \frac{\varepsilon''}{\varepsilon'}$, as well as the tangent of the angular difference between a phasor representing the

applied potential and a phasor representing free charge stored on the capacitor plates. In ratio form, the loss tangent is comparing the energy lost to the energy stored. Figure II.F.3 shows the angular difference modeled in a phasor diagram comparing the charge, voltage, and current.[18] The phasor is rotating about the origin at a frequency ω. The current and charge are out of phase, as a result of the current being the time derivative of the charge. The angle between the current and the voltage is φ while the loss tangent it based on the complement of this angle, $\tan(\delta) = \tan(90 - \varphi)$.

A loss tangent of zero means that the current and voltage are $\pi/2$ or 90º out of phase, meaning that all energy is stored. This would be an example of a perfect capacitive system. The other extreme is a system with no capacitive effects, where the real dielectric constant is zero, and thus the current and voltage are in phase with one another. This is a resistive system in which all energy put in is lost, dissipated into heat.

The loss tangent and the imaginary dielectric constant in Nafion contain characteristic resonance peaks that are a function of frequency and temperature. One of the more easily studied peaks is the gamma relaxation peak. It is called this because it is the third peak in a series, and it is observed in dry samples at approximately -40ºC, making it straightforward to study. Dielectric relaxation is generally studied at several set frequencies, over a changing temperature range. This technique is used to help insure that the response is noticeable above the normal background noise. Attempting to observe the sample at one temperature, with a changing frequency introduces more background effects, thus masking the materials response. Observing several of these data sets overlayed on one another shows that the temperature at which the

resonance occurs is different for each frequency. Thus, as the sample is heated, its microscopic properties change to the point that it resonates at a different natural frequency.

In order to analyze the effect of temperature on the resonant frequency, the gamma peak frequency is plotted on an Arrhenius graph. In this representation, the log of the peak frequency is plotted against the inverse of the temperature. The peak frequency is the maximum in the resonance for its corresponding temperature. A constant slope in an Arrhenius plot implies that the activation enthalpy of the dipoles is constant throughout the observed temperature regime. A linear slope on an Arrhenius plot means that the frequency is temperature dependent in the form $f_{\max} = f_0 e^{\frac{-E}{kT}}$. Where E is the activation enthalpy for the potential well surrounding each dipole, and k is Boltzmann's constant, and T is the temperature of the surrounding environment. The resonant frequency is f_{max}, and f_0 is a material-dependent coefficient.

Figure II.F.4 shows an Arrhenius plot of the gamma peak for Electrosprayed Nafion. It has a decreasing slope of the form $y = mx + b$. In this specific case: $b = \ln(f_0)$, $y = \ln(f_{\max})$, and $x = \frac{1000}{T}$. The slope has units of Kelvins. This can be achieved by defining m as $\frac{-E}{k}$. Thus, the slope and the intercept of the Arrhenius plot are defined as material properties of the sample.

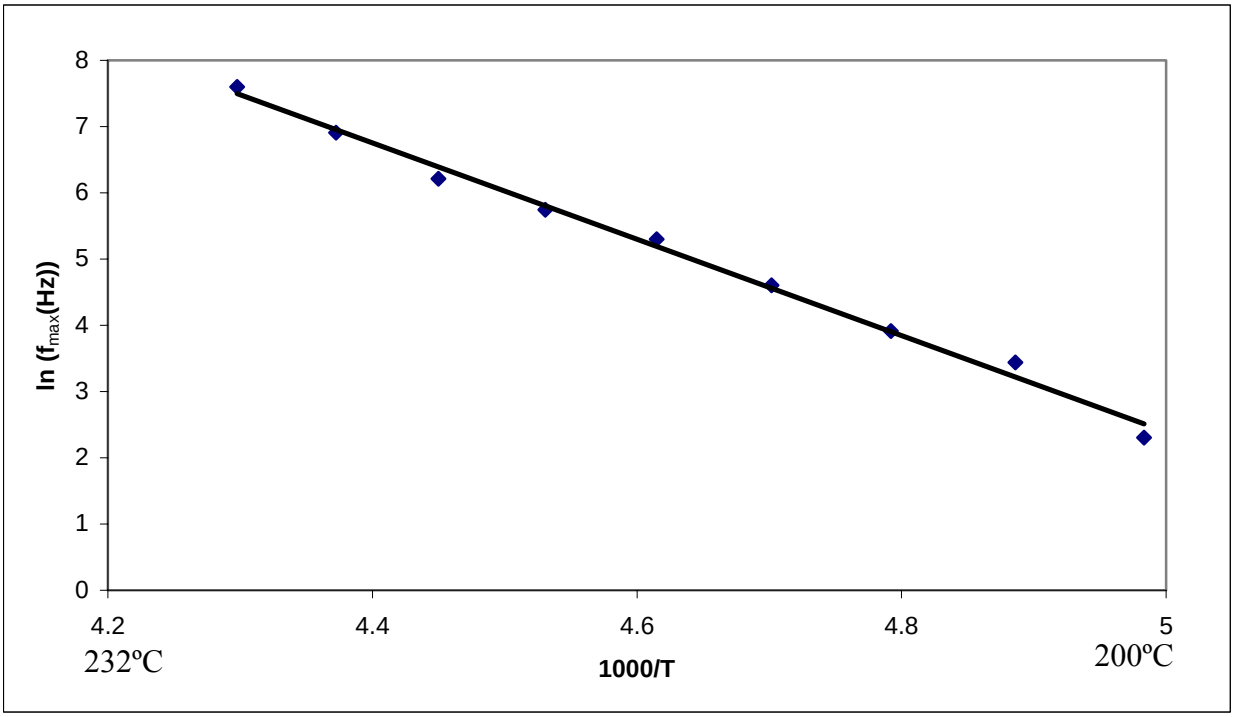

Figure II.F.4 Arrhenius Plot of Gamma Peak for Electrosprayed Nafion

In this study dielectric relaxation will be used to compare Nafion 117, and Electrosprayed Nafion, to verify that they are microscopically equivalent. Similar studies of the mechanically driven system using a process known as Dynamic Mechanical Analysis (DMA) have shown resonance peaks. DMA comparisons of Nafion 117 and Electrosprayed Nafion are planned as future studies of mechanical strength and relaxation; a summary of the process is provided in Appendix A.

G. Nuclear Magnetic Resonance

Nuclear Magnetic Resonance, NMR, is a powerful materials analysis tool for studying mass transport within a material. This tool is useful in the study of Electrosprayed Nafion and Nafion 117 membranes, because it allows the researchers to compare the movement of charge, as seen in the conductivity, with the movement of water. Colleagues at Hunter College, CUNY,

performed the NMR studies of Electrosprayed Nafion and Nafion 117. This information is included in this paper, as it contributes greatly to the understanding of the proton transport that takes place in Nafion membranes.

The Pulse Gradient Spin-Echo (PGSE-NMR) technique was used for the analysis in this project. This technique is used to measure the diffusion coefficient and the spin lattice relaxation time for the samples.[19] The diffusion coefficient allows for comparative responses between materials, as well as a classification of whether or not charge carriers are moving via the Grotthuss method or vehicular transport. In NMR, the diffusion coefficient can be thought of as the average rate at which water moves through the material. Technically the diffusion coefficient measures the motion of protons, both those bound to water and free charge carriers. There are many more water molecules in a wet sample, and each water molecule has two protons that can be observed in these measurements, and therefore, the diffusion coefficients are typically assumed to represent the motion of water. There is also a diffusion coefficient for charges, which can be found via the Nernst-Einstein equation, Eq II.G.1.

$$D_\sigma = \frac{kT}{q^2}\frac{\sigma}{N} \qquad \text{Eq II.G.1}$$

where N is the charge carrier density, T is the temperature of the sample, σ is the conductivity, k is Boltzmann's constant, and q is the charge of the carrier. This diffusion coefficient can then be compared to that found via PGSE-NMR. If $D_\sigma = D_{NMR}$ then the protons are being transferred on hydronium ions as is the case for vehicular transport, since the charge is moving at the same rate as the water. However, if $D_\sigma > D_{NMR}$ the protons are being conducted via the Grotthuss mechanism. This is because in the Grotthuss mechanism the charge moves through the material at a higher rate than the diffusion of water molecules.

Spin lattice relaxation times are a measure of energy loss within a system. When radio frequencies are applied to the system, the protons orient themselves to have the same spin direction. Spin lattice relaxation time is measured by using an RF pulse to perturb the spins of the molecules, and measuring the time constant for their return from the aligned state. The time it takes to recover from the perturbation is related to energy dissipated as heat, and provides insight into the small distance transport of protons.

PGSE-NMR measurements of diffusion coefficient consist of two pulses in the radio frequency band, interspersed with two pulses of a magnetic field gradient. It also allows the use of a narrower bandwidth receiver, thus reducing the background noise that can conceal the response. This method was developed by Stejskal and Tanner.[20] The spin magnetization of the atoms are aligned to the Z-axis, then pulsed with a 90º RF. This RF is one quarter of the period of the wave, and is used to reorient the spins into the X-Y plane. The magnetic field gradient is a magnetic field changing in intensity with respect to location. The magnetic field causes a precession of the spins. The changing intensity of the field means that the spins will precess at different frequencies depending on their location within the field. Thus, the phases of spins will no longer be aligned. A second RF pulse, of 180º, is used to flip the direction of the spins. The final magnetic gradient pulse forces the spin magnetizations to precess in the opposite direction as before, thus realigning the magnetizations. However, because self-diffusion is occurring within the material, some of the atoms are subjected to a different magnetic field, due to the gradient, than expected.[21] This results in an attenuation in the spin-echo response of the magnetizations when comparing the two values when the spins were aligned. The diffusion coefficient is related to this attenuation in spin magnetizations.[16]

III Materials and Instruments

The materials considered in this study are listed below. Each involve a different deposition technique for the Dupont polymer Nafion with a molecular weight of 1100. Nafion 117 is a commercially available polymer, while the Electrosprayed and cast Nafion are from a commercially available liquid Nafion and alcohol solvent. These two depositions were prepared at Virginia Commonwealth University, while the Nafion 117 was purchased directly from the manufacturer.

Nafion 117 – DuPont polymer membrane extruded at 7 mil thickness

Electrosprayed Nafion – Nafion deposited via an electrospray technique at Virginia Commonwealth University

Cast Nafion Film – Cast deposited polymer made from the chemicals used in the electrospray technique.

The instruments used in this study include three different pieces of equipment that measure the impedance responses of the materials, the sputter coater for sample preparation, and two different atmosphere control chambers. The impedance analysis instruments are useful over certain overlapping regimes, and the results have been compared to show that experimental results are not an artifact of a particular instrument.

Hewlett-Packard 4194A Impedance/Gain-Phase Analyzer

1255 Solatron Frequency Response Analyzer connected to a Solatron 1296 Dielectric Interface

Andeen CGA-83 Capacitance Bridge

Denton Vacuum Desk II Turbo Sputter Coater

ETS model 514 Automatic Humidity Controller using an ETS 5612C Ultrasonic Humidification System connected to a Humidity Control Chamber

Vacuum Atmospheres Company Atmosphere Control Chamber

IV Methods

In order for the sample to be tested it must be properly prepared[22]. The first step in the preparation of the sample was to sputter gold onto the membrane to establish a conducting contact point for the sample. The location of the gold sputtered contacts for an in-plane sample can be seen in Figure IV.1. It is important to note that the gold sputtered contacts were primarily along the wide flat surfaces of the sample, although it is highly probably that the gold coated part of the edges as well. After contacts were applied to both sides of the sample, it was dried and its mass determined. The mass of the gold was small in comparison to the mass of the sample. The mass of the sample is used in determining the weight percent of water in the sample. The dry-state mass is the baseline reading to which the others are compared, so the gold contacts must be sputtered onto the sample before determining the mass.

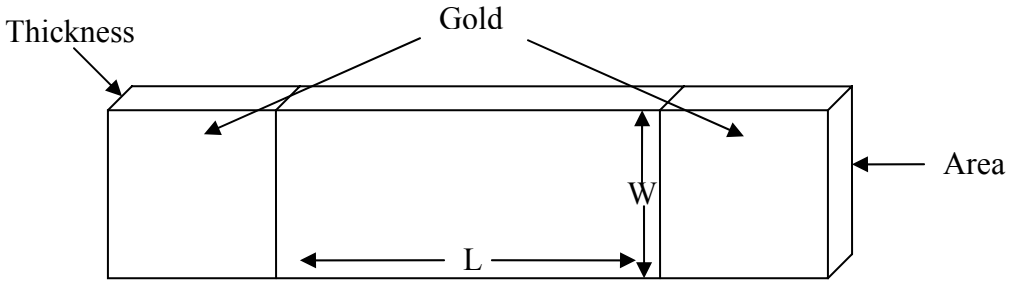

Figure IV.1 In-Plane Sample

For measurements concerning how the orientation of the membrane affects conductivity, the sample was prepared another way. The cross-plane sample is used to measure properties perpendicular to plane of the extruded or Electrosprayed Nafion. In Nafion 117, previous studies have shown that the extrusion process aligns the molecule backbones and side chains This may or may not be the same case in the electrospray, where the globules may be randomized molecularly compared to the extruded membrane. Figure IV.2 shows the location of the gold sputtered contacts for the cross-plane sample.

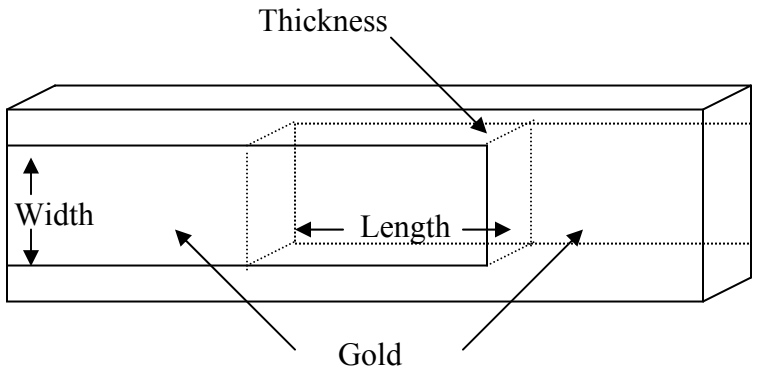

Figure IV.2 Cross-Plane Sample

These materials absorb water from the atmosphere; therefore, their water contents were adjusted by changing the relative humidity of their environment. Depending on the experiment, once the water content had stabilized the samples were either measured to determine conductivity as a function of water content, or hermetically sealed for Activation Volume measurements[23].

The relative humidity for the samples was set inside a controlled humidity chamber, a humidistat. This chamber has electrical feed-throughs to allow impedance analysis, so that their conductivity could be measured while in equilibrium. This is also the location in which they were hermetically sealed in order to set their water content prior to taking Activation Volume

measurements. The conductivity was calculated using the conductance and the dimensions of the sample; thus, these dimensions must be recorded at some time during the preparation of the sample. The cross sectional area for in-plane samples was taken to be the product of the thickness by the width, and the length was measured between the gold contact points. The volume of the sample is the part of the material that has not been covered during the gold sputtering. For cross-plane samples the volume was the center box covered on top and bottom with gold. Length and width measurements were taken via digital micrometers and calipers, while thicknesses were measured using a gauge stand with digital indicator.

Sample conductivity is measured as a function of water content at atmospheric pressure within the humidity-controlled glove box. Two samples of each of the three materials were examined. To minimize sample handling, one sample was evaluated for conductivity while the mass of the other was determined in order to extract the weight percent of water. The second sample was also measured in length to find the percent change caused by swelling. The relative humidity was adjusted in five percent increments within the glove box, and the sample was given at least half an hour to adjust to the new environment. This allows the water content to stabilize. Previous studies had shown that Nafion 117 easily achieved equilibrium within this time period, while Electrosprayed Nafion was observed over repeated measurements to verify this feature as well. The conductivity was then measured using either the Solatron or the Hewlett Packard frequency response analyzers for one of each of the three types of samples. Data plotted as one hundred percent relative humidity is found by wetting the samples with deionized water, while maintaining the chamber at 92% relative humidity. The humidity control chamber being used in this study could not maintain relative humidity higher than 92%.

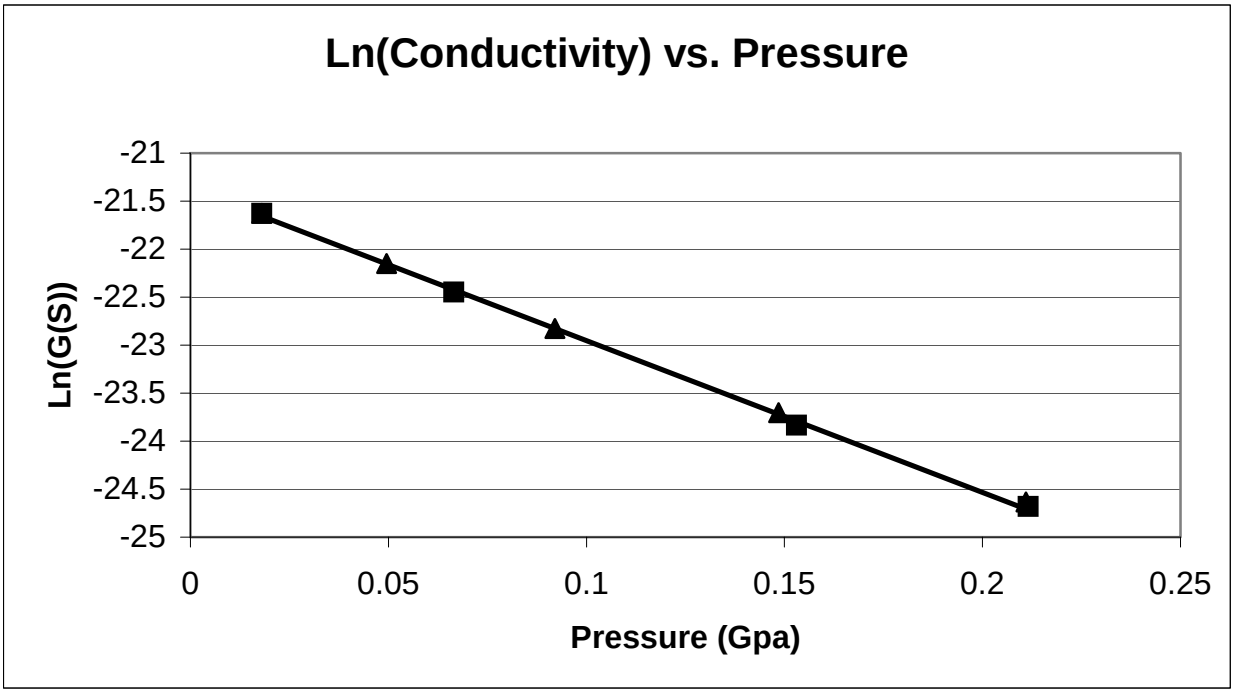

Figure IV.3 Sample Plot of Data Taken via a Hysteresis Loop:
■ - Descending Pressure ▲ - Ascending Pressure

The process of taking data both ascending and descending in relative humidity or pressures is known as completing a hysteresis loop. The hysteresis data plotted in Figure IV.3 is for the activation volume measurements requiring changing pressures, as opposed to conductivity and relative humidity. Both studies require the use of hysteresis loops to verify data; this loop was selected because of the ease in seeing the correlation of the two paths. In Figure IV.3, the squares represent the descending pressures, and the triangles represent the ascending pressures. Notice that there is no "history" dependence in this data. The reasoning behind making a hysteresis loop is to ensure that the data is repeatable. If there is a large discrepancy between the resistances found at two similar relative humidities, either there is a problem with the system, or the sample properties are "history" dependent. After a hysteresis

loop of relative humidity dependence was completed, the samples were swapped, and another data set collected.

In a study of the activation volume for these membranes, the samples were hermetically sealed at a selected water content. As shown in Figure IV.4, the sample was hermitically sealed inside a small length of Viton tubing. Viton was selected because of its flexibility and temperature stability while resisting the acidic properties of the Nafion. A small metal foil was bent around the edge of the tubing, and then a clamp was applied, sandwiching the tube, metal foil and sample into one tightly bound piece. This was done to both ends of the tube and sample. The metal foil had to remain in contact with the gold sputtered edges of the sample as well as with the metal clamp holding the outside the edge of the tube. Wires were attached to the clamps so that the circuit was completed through the clamp, the foil, the sample, the other foil, the second clamp, and out through the other wire. The resistances of the wires and clamps are negligible in comparison to those of the sample.

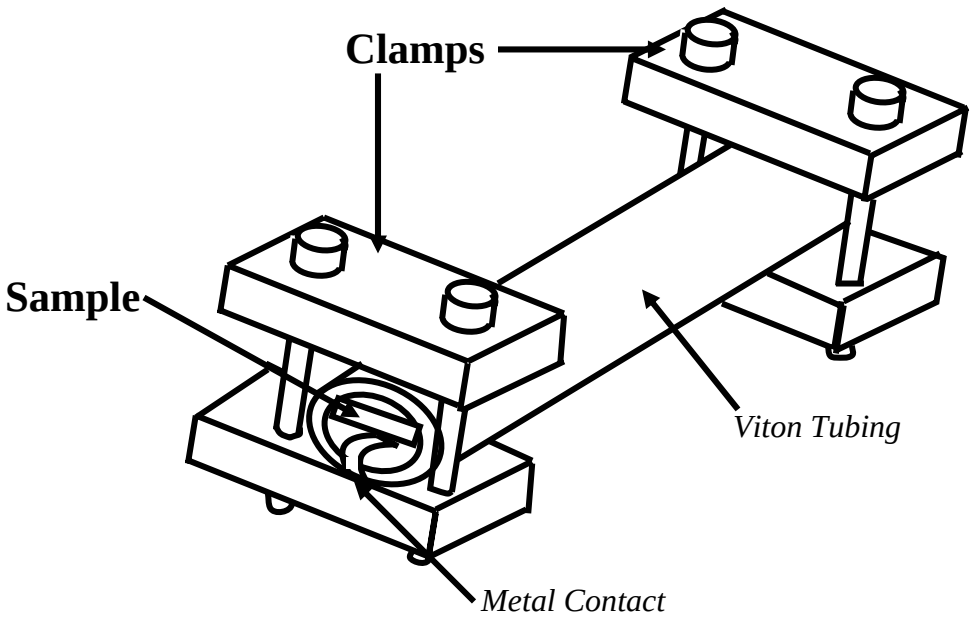

Figure IV.4 Hermetically Sealed Sample

The sealed sample was then placed inside the pressure vessel. The seal provided the dual roles of maintaining the water content of the sample, while also protecting it from the oil inside the pressure vessel. In this way the pressure vessel environment around the sample did not change anything except for the temperature and pressure of the sample.

In this experiment the samples were tested at various pressures, starting with a run at room temperature. The pressure was raised to about 2500 bars. The pressure vessel was given thirty minutes to equalize with the outside conditions. These thirty minutes were taken because although the sample was originally equalized, raising the pressure of the vessel and sample also raised the temperature. The thirty minute time period was verified by observing the equalization of temperature within the vessel after the pressure was adjusted. An impedance arc is measured so the bulk resistance could be determined, and after each such run the pressure was lowered in increments of 400 to 500 bars. After each increment, the system was again allowed to equalize, and then an impedance data set was collected. Once a minimum pressure of approximately 100 bars was reached, the pressure was raised again by 400 to 500 bars, allowed to equalize, and data was taken. The tests continued until a maximum pressure of about 2500 bars was again reached. Thus, the activation volume measurements were also taken as a hysteresis loop, of pressures, in order to better ensure repeatability of the data.

When taking activation volume measurements, there were many cases in which hysteresis occurred within the samples. Because this was not a consistent phenomenon it was viewed as an error in the method, and the data was discarded. It was found that if the samples spent too long under high pressure their conductivity would increase significantly for that pressure. Thus, for certain samples, the activation volume measurements had to be completed in about one day. This still allowed enough time between measurements for stabilization of the sample at each

pressure, but lessened the number of pressures that were tested within each loop. This change in the sample's conductance over long periods of time at pressure may be the result of acidic attack on the stainless steel foil and merits investigation. This would not be an increase of sample conductivity, so much as the creation of another conduction path in parallel to that of the sample, which would reduce the observed resistance.

To study the dielectric relaxation of the samples, samples were first gold sputtered, then dried in an evacuated chamber. Dimensional measurements were taken in a dry environment, and the samples were loaded into the testing cells. Next the samples were placed in an oven and heated to 380K for three weeks. This fully dries the samples to the point that the resonance peaks could be distinguished from the background. Measurements of the complex dielectric constant in Electrosprayed Nafion were taken using an Andeen CGA-83 Capacitance Bridge with a dielectric interface. Outputs from this equipment come in the form of C_P and $\frac{G_P}{\omega}$. These outputs can easily be converted to the forms $\varepsilon' = \frac{C_P}{C_0}$ and $\varepsilon'' = \frac{G_P}{\omega C_0}$. Measurements taken over a range of temperature and frequency were plotted to show the relation between resonance frequency and temperature.[13]

Samples of Electrosprayed Nafion were sent to colleagues at Hunter College, CUNY, where they were studied using the Pulse Gradient Spin-Echo technique. This involved suspending the samples in a sealed test tube over water to set their water content in a 100% relative humidity environment. The samples were then studied using a Chemagnetics CMX-300 spectrometer for their diffusion coefficients and spin lattice relaxation times. The instrument was calibrated for water. These techniques were later used to observe NMR differences in the

orientation of Nafion 117. The results of this study prompted the orientation comparisons for both Nafion 117 and Electrosprayed Nafion.

To study these orientation effects in conductivity, samples were prepared as described above for in-plane and cross-plane measurements of the membranes. The samples were then dried, and dimensional measurements were recorded in situ. Conductivity measurements in a humidity controlled chamber, as well as activation volume measurements in dry conditions were taken for the samples. As a result of conductivity differences between in-plane and cross-plane transport being found, orientation effects on Nafion 117 activation volume and Electrosprayed Nafion conductivity were measured.

These activation volume measurements for Nafion 117 were meant to investigate the previously published data in which the dry measurements were taken across the plane of the sample, at elevated temperature, and wetter samples were measured via the in-plane method. Large resistances in dry in-plane samples (>1 T-ohm) and instrument limitations forced the use of the cross-plane geometry in these previous studies. The previously published data did not distinguish between the two measurements. Studying the effects of orientation of the membrane on activation volume allows for an examination of the way proton transport may be affected by the alignment of the polymer molecules.

V Results

A. Water Absorption and Dimensional Stability:

Proton transport in Nafion is known to be a strong function of water content. Therefore, the first feature examined for Electrosprayed Nafion was the water absorption and dimensional changes that occur as a result of exposure to atmospheric humidity. These measurements are a

comparison of Nafion 117, Electrosprayed Nafion, and a cast Nafion film made from the pre-electrospray solution of Nafion and an alcohol solvent. These samples were placed in a controlled humidity chamber and evaluated at various relative humidities. The mass and dimensions were measured in situ while the humidity was held constant.

Figure V.A.1 is a comparison of the water content in weight percent at various relative humidities for Electrosprayed Nafion and Nafion 117. The last data points plotted at 100% relative humidity point are actually in a saturated condition, where the samples were wetted with deionized water. Two interesting features from this data are noted. First, the response for the two materials, up to approximately 92% relative humidity, are highly similar. 92% is the maximum controllable relative humidity, and it corresponds to a 15 wt-% water uptake in both samples. Thus we see that Electrosprayed Nafion behaves like Nafion 117 when subjected to the same environmental moisture at room temperature. Second is the jump in weight for the Electrosprayed Nafion at saturated conditions. While the ability to hold water is an important feature when used in fuel cell applications, the location of the additional water in saturated Electrosprayed Nafion has not been determined, and therefore, the importance of this additional water is not known.

Figure V.A.1 includes two different methods of introducing water into the membrane material. In actual fuel cell usage, water is introduced via a third method. It is created at the boundaries and then must diffuse throughout the membrane. Since previous studies have shown that Nafion rapidly transports water within the membrane, it is assumed that the response of the membrane to this third method of water introduction will be similar to that found for the methods used in laboratory conditions. Of overall importance in this plot is the comparison of water contents for Nafion 117 and Electrosprayed Nafion.

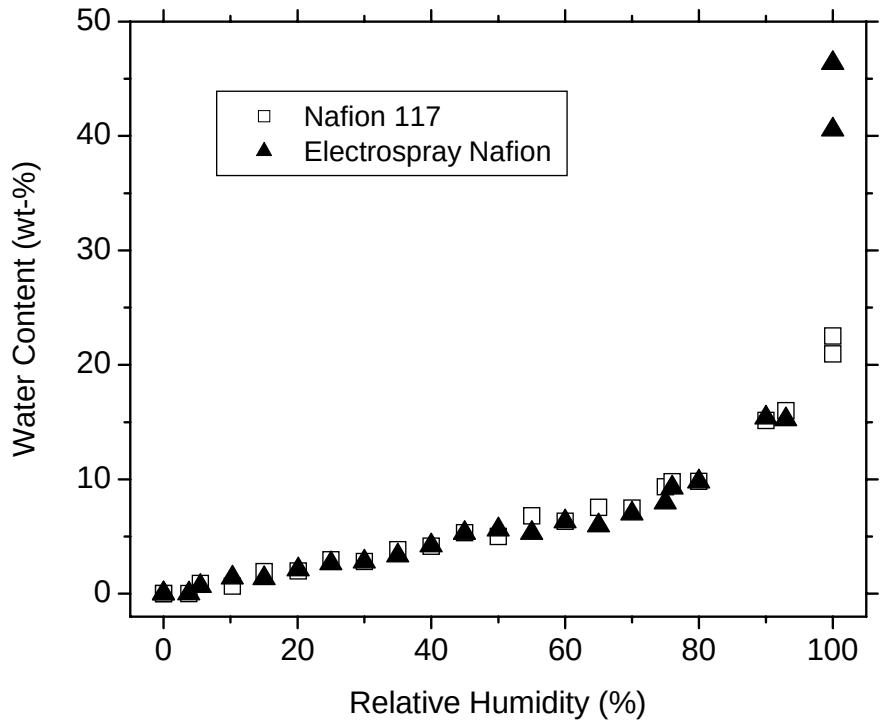

Figure V.A.1 Water Content vs. Relative Humidity

In dry conditions, the Electrosprayed Nafion membrane is fragile when compared to the extruded 117 membrane. This made measurements difficult as the sample tended to fracture when the relative humidity was less than 10% in the control chamber. This was not an issue at higher relative humidities. Concerns regarding the material strength of the electrosprayed membrane in dry conditions must be further investigated using DMA. For a more thorough discussion of DMA, see Appendix A.

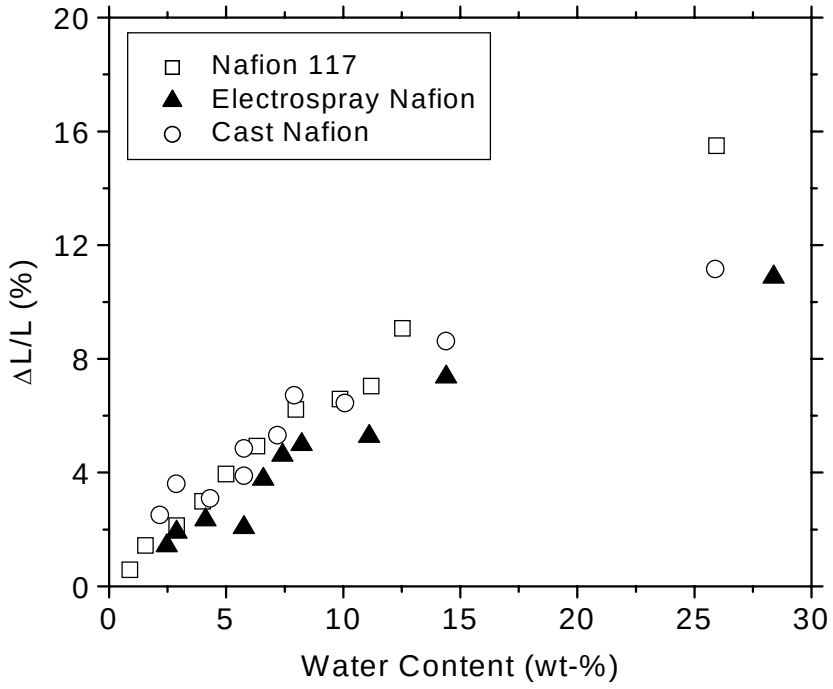

Figure V.A.2 Change in Length vs. Water Content

As the polymer absorbs water, the samples swell in all three dimensions. In Figure V.A.2 the proportional change in length for the various samples at different water weight percents are compared. From approximately 2 to 15 weight percents the dimensional changes follow a linear pattern. The large gap in data points between 15 and 25 wt-% water is accounted for by the large increase in water content in going from 80% relative humidity to 92%. The gap in this data arises because the water content between the two relative humidities cannot be finely controlled. This data shows that there is a general trend that increasing water content leads to sample swelling. Using the trends for the three samples, the dimensions can be appropriately adjusted for use in converting conductance to conductivity. The sample dimensions for each water

content are important, in that they provide more specificity in the determination of conductivity values. This estimation is used in order to avoid over handling of the samples.

The uncertainty in the dimensional measurements is estimated to be 3% for each data point; the standard deviation about the best fit line was taken to be the uncertainty. This error comes from the difficulty inherent in using digital calipers to measure the small samples inside of the glove box environment. A difference of a few tenths of a millimeter in measuring the length can have significant effects for small samples when converted into a fractional percent of the length. This information will preclude the need to measure sample dimensions on subsequent experiments which require knowledge of dimensions. Sample length, width and thickness will be measured in the dry state and estimated at other water contents.

The primary purpose of this measurement was to allow an estimate of length as a function of water content. A fit of the data in Figure V.A.2 will be assumed to approximate the swelling of each dimension as a function of water content. Minor non-uniformities in the film made it difficult to accurately determine swelling for thickness and width, and therefore it is assumed that all three dimensions swell equally. This accounts for an increased cross sectional area through which to pass protons, as well as an increased distance over which the ions must be transported. Both of these values are crucial in converting the bulk resistance of the membrane into a conductivity.

B. Conductivity Comparisons

Conductivities for extruded, electrosprayed, and cast Nafion are plotted versus their corresponding water weight percent in Figure V.B.1. Note that over a relatively small increase in water content, from 0 to 10 wt-% water, the conductivity of the sample increases by approximately 5 orders of magnitude. Beyond this point, the change in conductivity tapers off to

a change of one order of magnitude despite a 20 to 40 wt% water gain. The conductivity of Electrosprayed Nafion is consistent with the Nafion 117 data within error, with the saturated state of electrospray following the trend of the other high water content data. Once again, the large gap in the data is due to the change between 92% relative humidity and saturation.

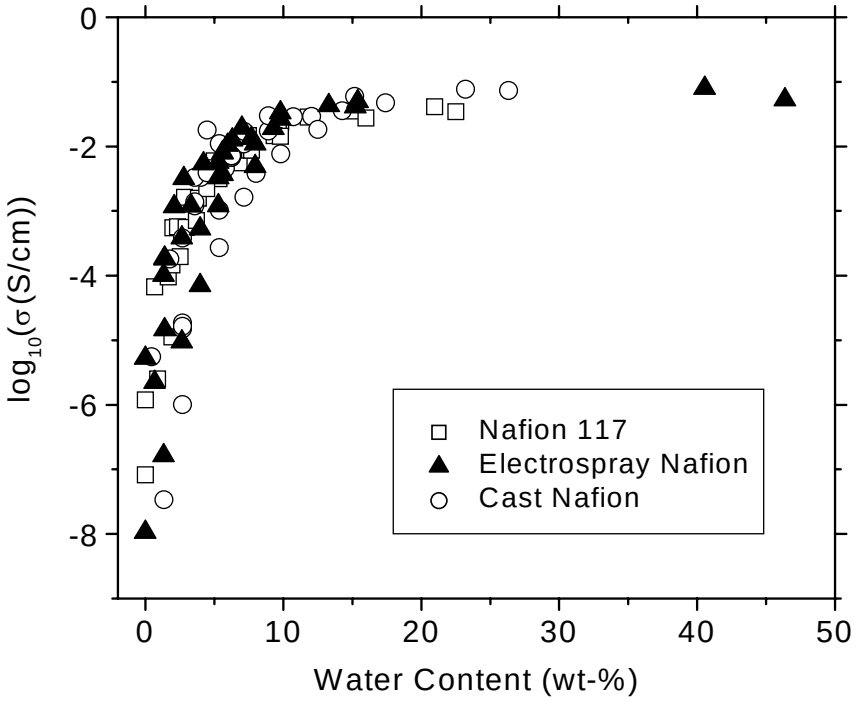

Figure V.B.1 Conductivity vs. Water Content

Uncertainties in this data arise from a number of sources. The first source is the difficulty in accurately measuring sample dimensions, as described previously. This difficulty is more that human sloppiness, it comes from the fact that the edges of the sample are never perfectly straight, and the gold sputtered boundaries do not evenly match up, or form a perfect rectangle. Also, the thickness of the samples has a good deal of uncertainty, especially in the case of the electrospray, where the different globules have coalesced to create varying

dimensions within the sample. The bulk resistance has an inherent uncertainty associated with fitting the complex impedance arcs.

Uncertainty in the impedance arc intercept results in a corresponding resistance uncertainty of approximately ±5%. This is due to distortion in the impedance arcs. Samples seldom create a complete arc, with a second intercept, as the electrode blocking effect begins to swamp the response. The uncertainty was found by comparing the different fitting techniques for finding the bulk resistance. The point in which the complex impedance plot displays prominently more electrode blocking than impedance arc effects is never a fixed value on the arc. Figure V.B.2 shows an example impedance plot in which the majority of the arc is still prominent. Figure V.B.3 is an impedance plot in which nearly half of the arc has been distorted by the electrode blocking effect.

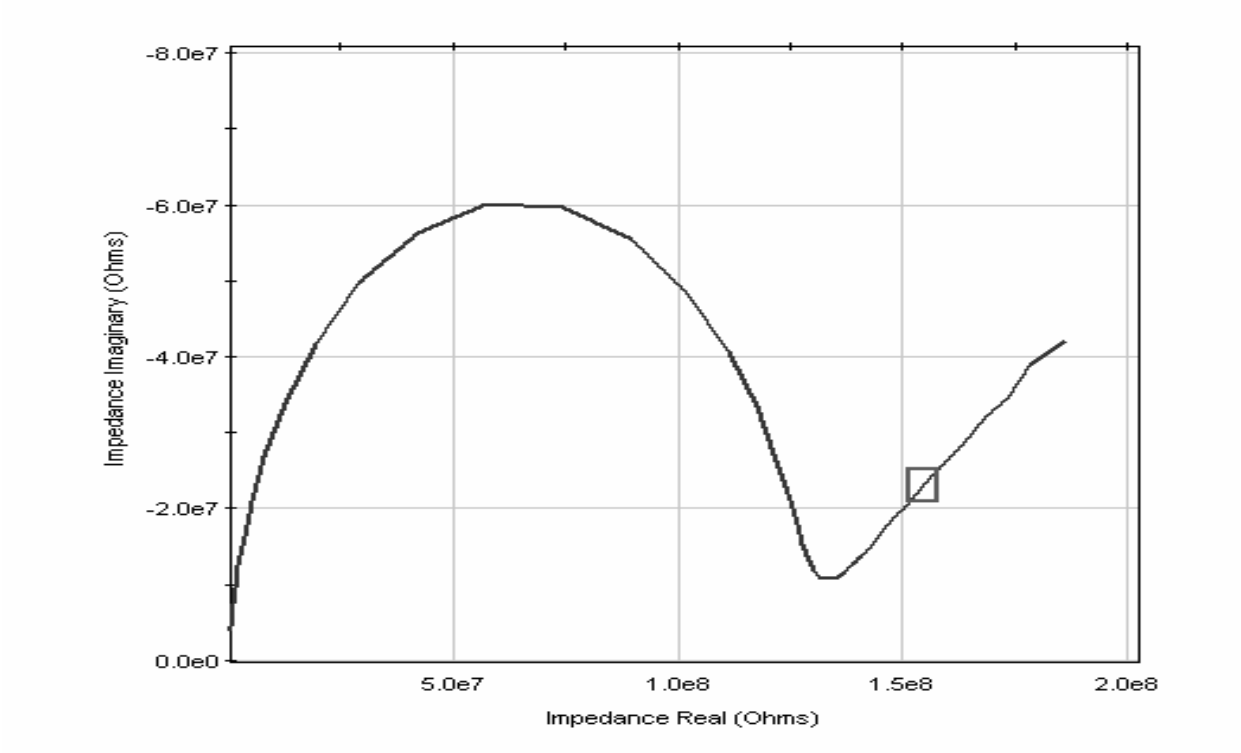

Figure V.B.2 Impedance Arc with Minimal Electrode Blocking

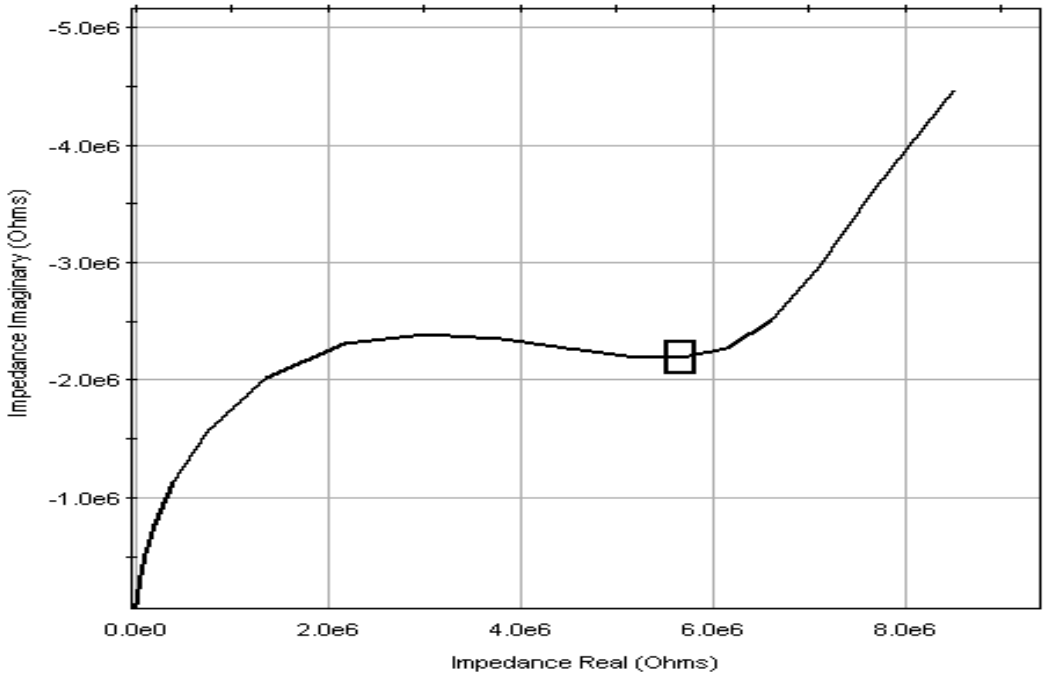

Figure V.B.3 Impedance Arc Distorted by Electrode Blocking Regions

The electrode blocking region effectively operates as a parallel plate capacitor in the sample. As the sample dimensions change, so does this capacitance, thus altering how it interacts with the region of the impedance arc. We can treat the electrode as if it were a generic parallel plate capacitor where, $C = \frac{\varepsilon A}{d}$. As the sample volume changes between the gold contact points, the electrode blocking capacitance changes as well. To attempt to control the uncertainty introduced by these changes, the researchers were consistent in the technique used to find the intercept. The two techniques most commonly used were to take the intersection of the electrode effects line and that of the arc as being the bulk resistance, or to use the symmetry of the arc to find the intercept.

The equation to find the conductivity has four uncertain factors, being multiplied or divided. In an equation of either the form $A = BC$ or $A = \frac{B}{C}$ the fractional uncertainties add as $\frac{\Delta A}{A} = \frac{\Delta B}{B} + \frac{\Delta C}{C}$. The conductivity equation is $\sigma = \frac{l}{Rwt}$, where *R* is the resistance, and *l, w* and *t* are the dimensional measurements. The uncertainties of 3% in each of the dimensions, and 5% for the measurement of the resistance add to a total uncertainty for the conductivity of roughly 14 - 15%. On the logarithmic plot this uncertainty is generally covered by the large size of the markers. This uncertainty is well within acceptable limits for this study, as it easily allows for a determination of the trend of the data, and a comparison of the deposition techniques.

C. Dielectric Relaxation

Dielectric relaxation data was taken for Electrosprayed Nafion in order to compare its microscopic properties with those previously published for Nafion 117. The samples were prepared as specified in the Methods section. Figure V.C.1 shows that a dielectric loss peak appears, and that it is both frequency and temperature dependent. This is consistent with results for Nafion 117, in which such peaks appear at or near similar temperatures for applied fields oscillating in the audio range.

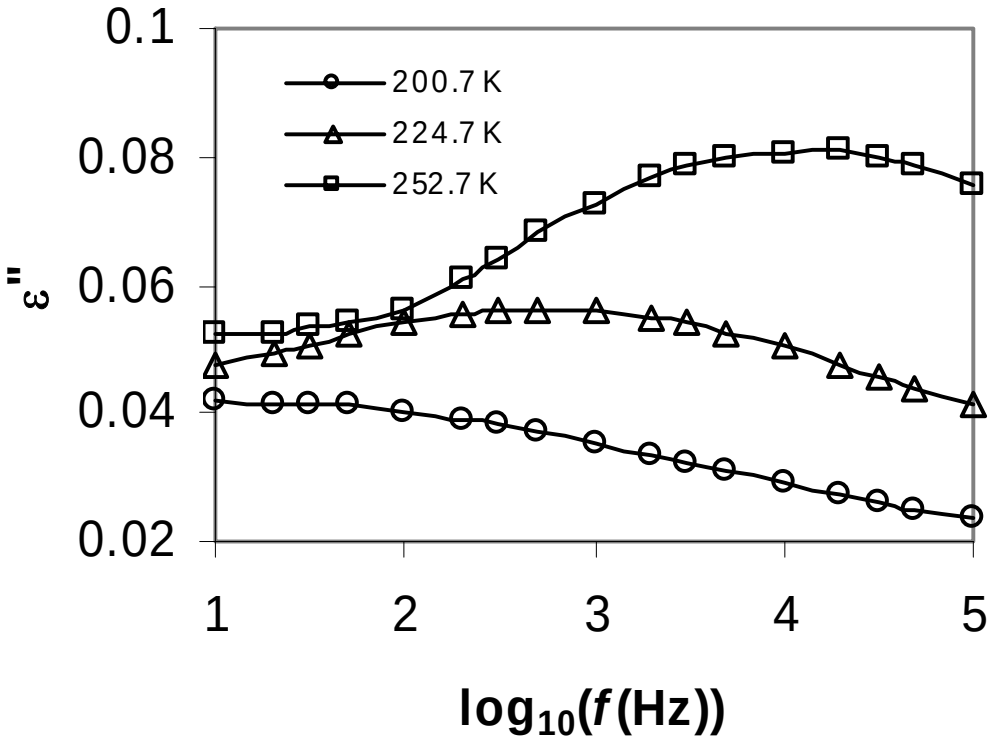

Figure V.C.1 Complex Dielectric Constant for Electrosprayed Nafion

In order to numerically verify that Electrosprayed Nafion has similar dielectric response to that of Nafion 117, the third or gamma peak was analyzed for Arrhenius behavior. This is shown in Figure V.C.2, where the peak frequency is plotted against the inverse temperature at which each peak occurs. As discussed in the background information concerning dielectric relaxation, a constant slope in an Arrhenius plot means that there is an activation enthalpy for the dipoles in the system.

$$f_r = f_0 e^{\frac{-E}{kT}} \qquad \text{Eq V.C.1}$$

Transformed for the Arrhenius plot:

$$\log(f_r) = -\frac{E}{kT} + \log(f_0) \qquad \text{Eq V.C.2}$$

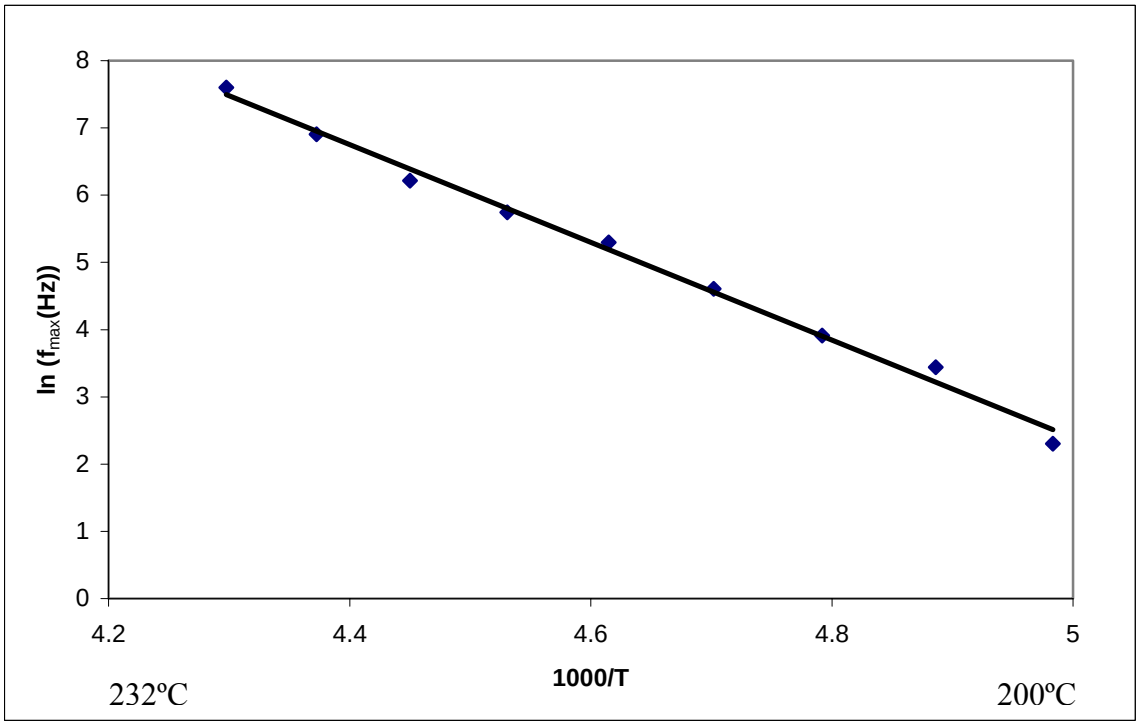

Figure V.C.2 Arrhenius Plot of Gamma Peak for Electrosprayed Nafion

For the results in Figure V.C.2, E = 0.63eV and $\log(f_0)$ = 16.8. These values are well within the uncertainty for equality with the reported values for Nafion 117 of E = 0.57eV and $\log(f_0)$ = 15.9.[10] Uncertainties in determining the peak frequency may be attributable to minute changes in water content for Electrosprayed Nafion. It is difficult to fully dry Nafion, and so water clusters may still exist around the sulfonate group affect the relaxation parameters. The 10% difference between the Electrospray values fit parameters and those of Nafion 117 are within the uncertainty of the measurements.

D. Activation Volume

Figure V.D.1 shows comparative studies for activation volumes of Electrospray Nafion and data previously published for Nafion 117.[15] The Electrospray data follows the same general trend as shown in the Nafion 117 data, thus implying that proton conduction occurs by the same means for both materials. There are several important features to note in this graph. The first is that the Nafion 117 data is relatively constant above 5 wt-% water. Second, below 5 wt-% there is a sharp increase in activation volume with decreasing water content. The 0 wt-% point for Nafion 117, was actually measured across the plane of the sample and at an elevated temperature of 50ºC. The studies of orientation effects on activation volume, in section V.F will investigate whether this change in measurement technique has an effect on the results.

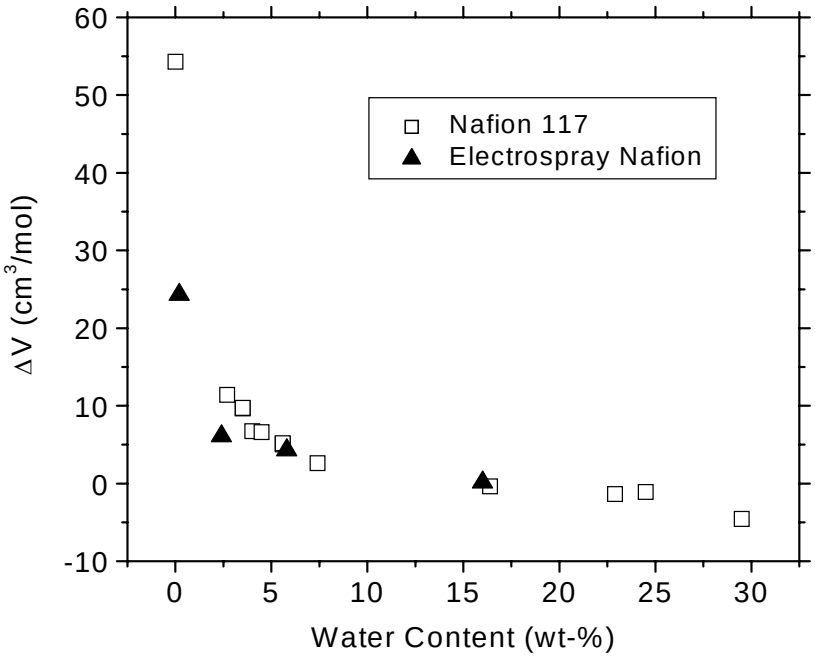

Figure V.D.1 Activation Volume vs. Water Content

Only four measurements were taken for activation volumes of Electrospray Nafion. This is because the new samples from Virginia Commonwealth University were considerably thinner than the samples used in the initial experiment. This made them highly susceptible to tearing when being hermetically sealed, especially for dry environments, where the electrospray is significantly more brittle than the Nafion 117.

The high activation volumes for dry Nafion polymers is indicative of side chain motion within the sample. This can be visualized as the side chains physically moving in order to transfer protons. The Grotthuss mechanism and vehicular transport correspond to lower activation volumes. Therefore, as water is added, the proton transport switches from a conduction means of side chain motion to either the Grotthuss mechanism or vehicular transport. This is somewhat intuitive, since both these means of conduction require the presence of water.

Notice that the scale on the vertical axis for the activation volume shows that measurements recorded for high water content samples of Nafion 117 fall into the negative regime. This is indicative of proton transport in water. This means that as the charge carrier passes through the medium, the volume actually shrinks, as the molecules are drawn to the charge by their polar nature.

Vehicular transport and the Grotthuss mechanism are not mutually exclusive phenomena within the sample. The most likely situation is that both are taking place at the same time, with one of the two methods being accountable for the majority of proton conduction. Determining whether or not vehicular transport of protons, or the Grotthuss mechanism is primarily responsible for the conduction in wet samples can be accomplished by comparing conductivity results with a study of Pulse Gradient Nuclear Magnetic Resonance.

E. Nuclear Magnetic Resonance

Electrospray Nafion samples were sent to Hunter College in New York to be studied via Pulse Gradient Nuclear Magnetic Resonance. The results of this research are included here as they help in gaining an understanding of proton transport. Also, NMR provides a useful way of exploring some of the microscopic properties of the samples. A complete comparison of Electrospray and extruded Nafion must take into account both the bulk and molecular characteristics of the material.

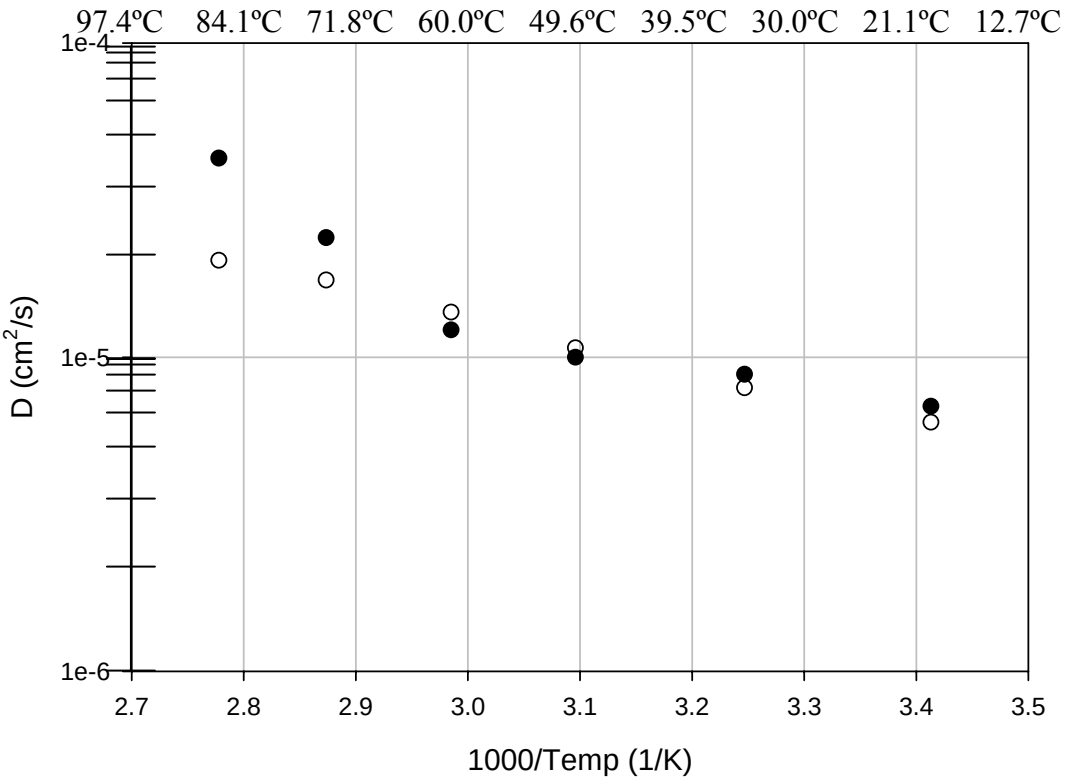

Figure V.E.1 Diffusion Coefficients: Electrospray Nafion: • Nafion 117: ∘

As seen in Figure V.E.1, the diffusion coefficient for Electrospray Nafion and Nafion 117, in the temperature range from 20 to 62ºC, correlated within the uncertainty of the measurements. Above 62º however, the Electrospray had a 30 to 70% higher diffusion

coefficient than that of the extruded polymer membrane. This may be related to the increased water absorption of Electrospray Nafion in saturated conditions. Diffusion coefficient measurements were taken at 100% relative humidity, and are plotted in Figure V.E.1.

A comparison the diffusion coefficients found using NMR with those obtained from the Nernst-Einstein equation, $D_\sigma = \frac{kT}{q^2}\frac{\sigma}{N}$, is used to determine whether protons are being transported primarily via the Grotthuss mechanism or by vehicular transport. Using the conductivity for the samples at 92% relative humidity, room temperature, Boltzmann's constant, and a number density of one charge carrier per atom, the D_σ was found to be 10^{-5}. This value is within the uncertainties of both measurements and indicates that vehicular transport is the primary mechanism of proton conduction at room temperature for wet environments.

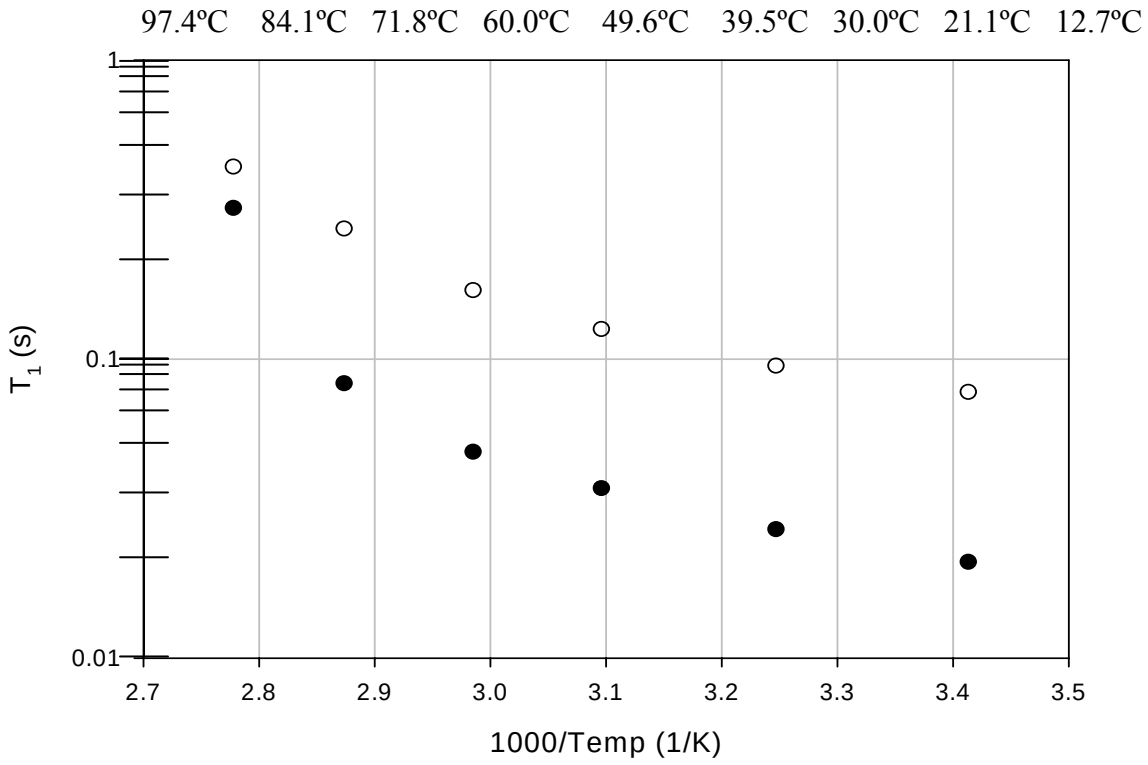

Figure V.E.2 Spin Lattice Relaxation Times: Electrospray Nafion: • Nafion 117: ∘

Figure V.E.2 shows a comparison of the spin lattice relaxation times for Electrosprayed Nafion and Nafion 117. There are two features to note in this figure. The first is that for the majority of temperatures, the two materials have parallel slopes. This is indicative of a similar response to the environmental conditions. As the temperature is increased from 22 to 62ºC the change in the materials response is the same. The second important aspect is that the spin lattice relaxation times for Electrosprayed Nafion are significantly less than those for Nafion 117. In reference 10, Greenbaum and Suarez at Hunter College interpret this to imply that for transport over short distances, the electrosprayed samples actually have restricted motion of the protons, and therefore a difference in short range molecular motions.

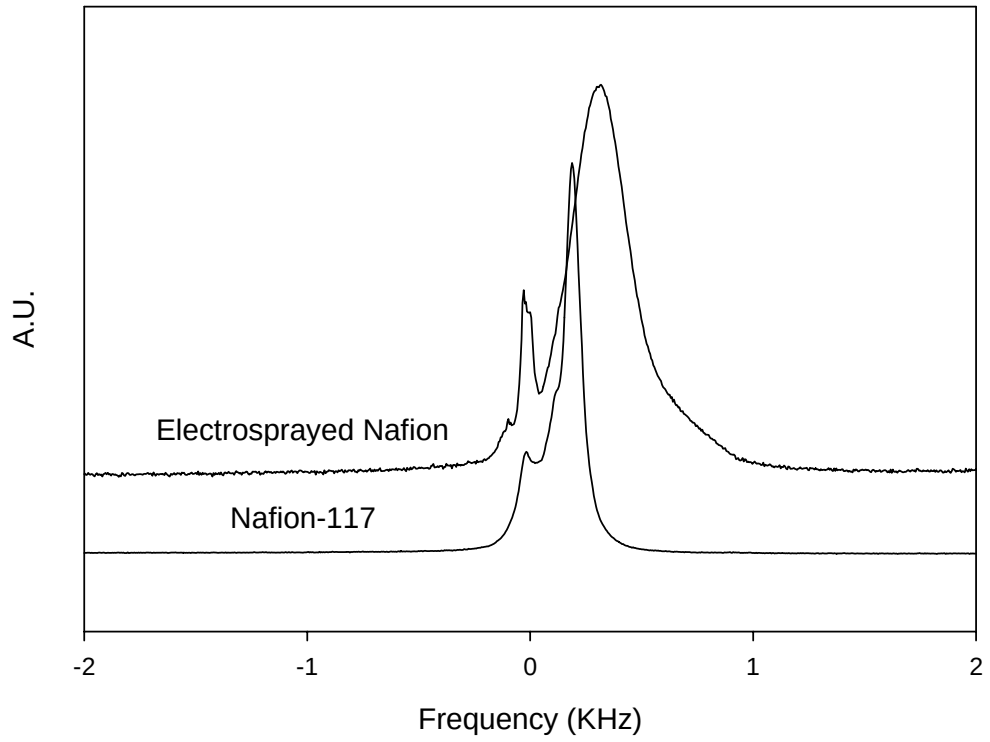

Figure V.E.3 NMR spectra at 20º C for Electrospray and extruded Nafion

Figure V.E.3 further substantiates these results. This plot compares the proton NMR data at 20ºC for the two materials, measured in arbitrary units. Notice the broader spectrum for the Electrospray Nafion. Greenbaum and Suarez at Hunter College state that this is also indicative of the more restrictive short range molecular motion, and therefore the lower spin lattice relaxation times.[10] Thus, Figures V.E.2 and V.E.3 are indicative that over a short range, there is a difference in molecular motion, with Electrospray Nafion being more restrictive than Nafion 117. However, Figure V.E.1 supports the conclusion that Electrospray Nafion and Nafion 117 have similar transport over long distances.

While studying the differences between Electrosprayed Nafion, and Nafion 117 at Hunter College via NMR, it was noticed that the orientation of the samples affected their diffusion coefficients. Nafion 117 was then studied to see how the orientation of the sample affected the diffusion of water within the material. Figure V.E.4 shows the results for the measurements of the diffusion coefficient at 20% water content for the samples.[24]

These results show a temperature range of 20 to 87ºC for a 100% relative humidity extruded Nafion sample suspended over water. It's important to notice that the measurements are taken in-plane, cross-plane, and a random mix of the two. The random sample always falls somewhere between the in-plane and the cross-plane. The in-plane sample is consistently 20% higher than the cross-plane diffusion coefficients. This means that there is a 20% greater ease in the flow of water molecules within the sample.

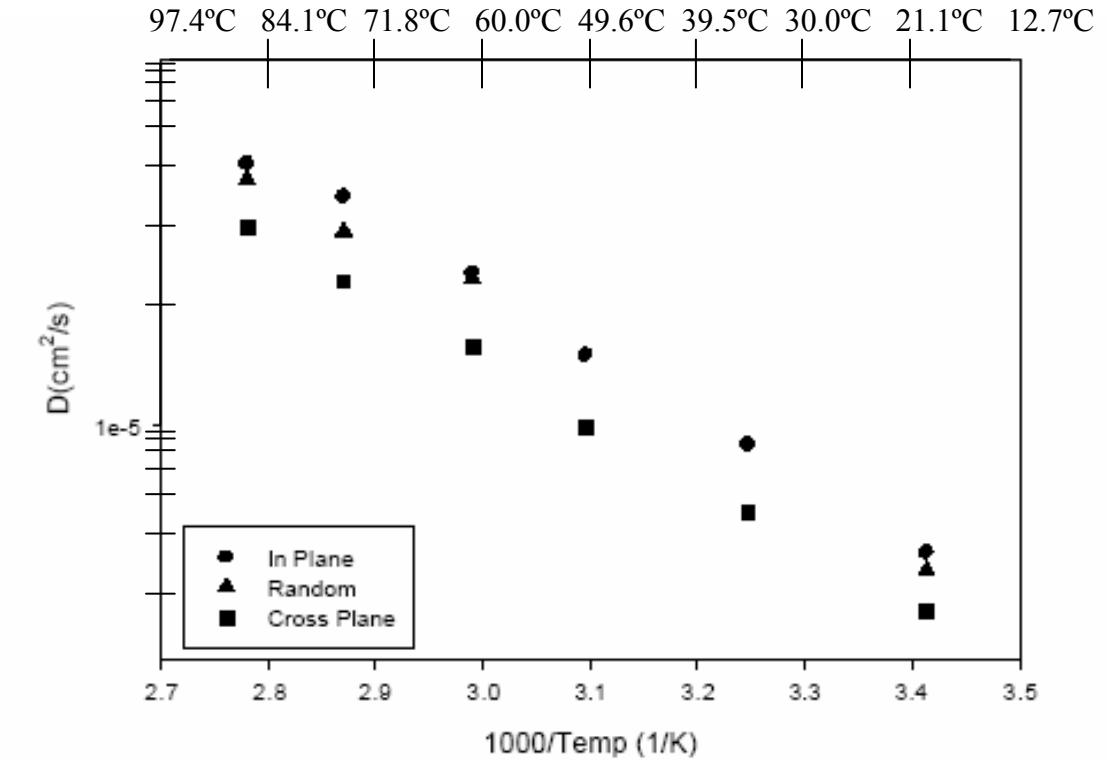

Figure V.E.4 Orientation Diffusion Coefficients for Nafion 117

These measurements may have a great significance on the understanding of proton transport in Nafion membranes. It is a fact that the extrusion process aligns the molecules, but it has not been shown that this has any effect on charge or water motion within the materials. The results of the research at Hunter College prompted an investigation of the conductivity differences between the in-plane and cross-plane measurements for Nafion 117.

F. Orientation Effects on Conductivity

Orientation effects in Nafion 117 may provide a significant clue to the proton transport properties, while also providing a useful comparison to Electrospray Nafion. In a fuel cell using Nafion 117 in the MEA, membrane conduction takes place across the plane of extrusion. This is done so that protons must only be passed over a small distance, since the resistance to charge carrier motion is directly dependent on the distance traveled. Also, it allows for a greater area, so

that for a given current density, the total current of the system increases. This provides increased availability of power for a load.

The orientation effects in conductivity and activation volume were studied for Nafion 117. The samples were prepared as described in the methods section for both in-plane and cross-plane samples. Conductivity or activation volume measurements followed the hysteresis loop pattern described earlier, in order to eliminate any history dependent effects in the measurements. This is especially important at high pressures, where long term exposure to pressure presents an irreversible change in the observed parameters. For studies of conductivity versus relative humidity of the surrounding environment, it was important to let the samples adjust to atmospheric conditions inside the chamber for at least 24 hours, as water absorption for the cross plane sample is hindered by the gold sputtered surface.

Figure V.F.1 shows the base 10 logarithm of the conductivity plotted against the chamber relative humidity for Nafion 117. This data shows a correlation of the conductivities at relative humidities higher than 12%, with over two orders of magnitude difference for the drier samples. This means that there is a significant difference in conductivity for the cross plane samples in dry conditions. Since this is not the first plot of conductance as a function of water content, it raises the question of why this was not observed in Figure V.B.1. There are several significant differences between Figure V.F.1 and Figure V.B.1, which is also a plot of the log base 10 of conductivity. First, the horizontal axes are different between the two graphs; Figure V.F.1 compares the conductivities to the relative humidities at which the measurements were taken, while Figure V.B.1 compared the conductivities to the wt-% water. The scales used in this study did not have enough resolution to accurately determine small changes in water content in extremely dry environments, and therefore these conductivities cannot be plotted against their

wt-% water. Figure V.F.1 shows significantly lower conductivities for both the in-plane and the cross-plane measurements, because all data in the figure are for samples with less than 4 wt-% water. This corresponds to the extreme left-hand edge of Figure V.B.1.

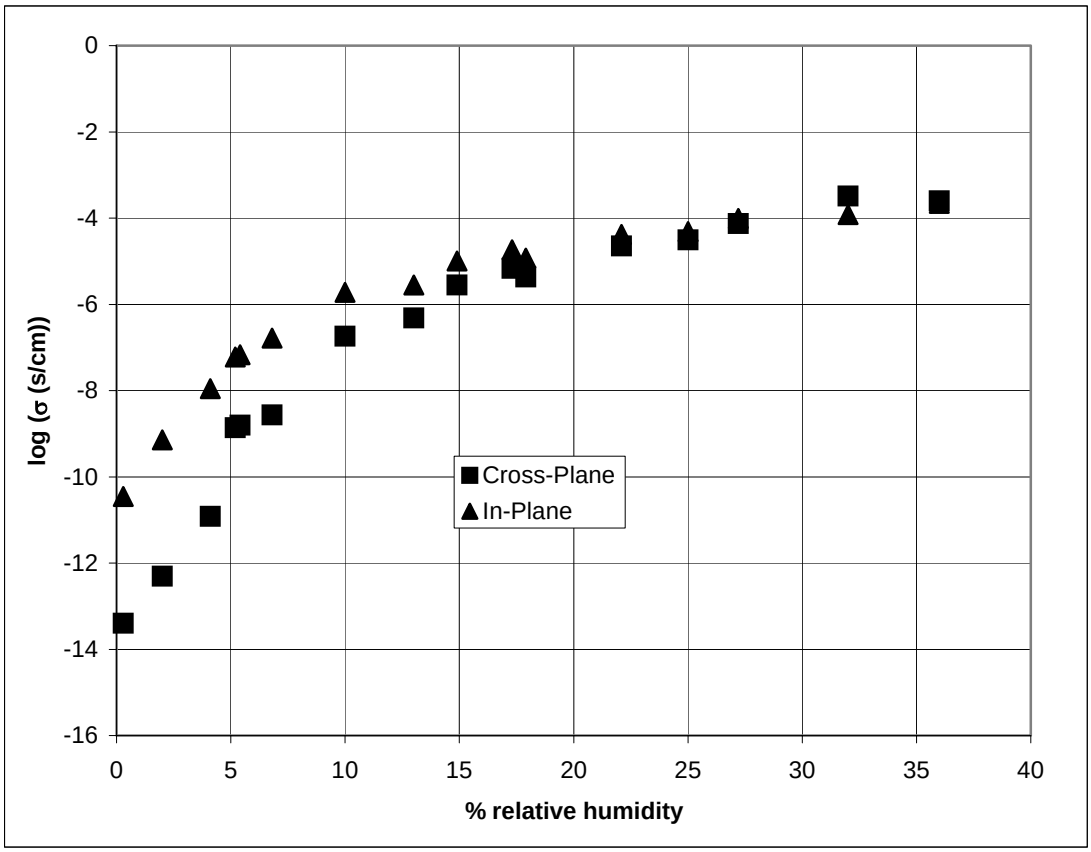

Figure V.F.1 Orientation Effects on Conductivity for Nafion 117

In the investigation of orientation effects of the conductivities only environments drier than 40% relative humidity could be studied. This was the limit at which the impedance analysis equipment was able to define an impedance arc for the cross plane samples. Since, $R_B = \frac{l}{\sigma A}$ where l is the length of the conduction path and A is the cross sectional area, dimensions play a large role in determining the bulk resistance. The ratio of length to cross-sectional area for cross-plane samples has 3 orders of magnitude difference when compared with

in-plane samples. Thus, the cross-plane conductance, $G_B = \frac{1}{R_B}$, is much smaller than that in in-plane measurements. This also means that the frequencies required for an impedance arc to be observed in cross-plane samples are higher. Forty percent relative humidity proved to be the limit at which the highest frequency impedance analyzer, the Hewlett Packard 4194A, could operate and show an arc. Beyond this limit, electrode effects obscured the impedance arc.

The extrusion of Nafion 117 is known to align the polymers such that the fluoro-carbon backbones are all facing in a similar direction. This data implies that the alignment in Nafion 117 may lead to easier proton conduction along the in-plane direction. The aligned backbones may also be the cause of lower conductivity for cross-plane measurements. This is because the hydrophobic nature of the backbone may interfere with water transport in dry conditions such that proton conduction is significantly affected. Cross-plane conductivity is significantly lower than in-plane for dry membranes; this can be critical in the use of Nafion in a PEM fuel cell.

Figure V.F.2 shows a comparison of conductivities for Electrosprayed Nafion and Nafion 117 at different orientations. This is the same Nafion 117 data shown in Figure V.F.1. It is important to note on this plot that the Electrosprayed Nafion has significantly higher conductivities in the driest environments. This may be related to the high water content absorbed in a wetted state and is potentially due to differences in the polymer morphology. This suggests that Electrosprayed Nafion may be a stronger candidate than Nafion 117 for use in fuel cells in dry conditions.

Electrosprayed Nafion does not show any orientation related effects. Although the in-plane measurements are slightly higher than those for cross-plane, they fall within the uncertainty for the measurements. However, for Nafion 117, there is a clear separation of

conductivities, as well as a difference of over two orders of magnitude. The fact that Electrosprayed Nafion does not show any orientation effects in dry environments supports its selection as a better candidate for PEM fuel cells than Nafion 117.

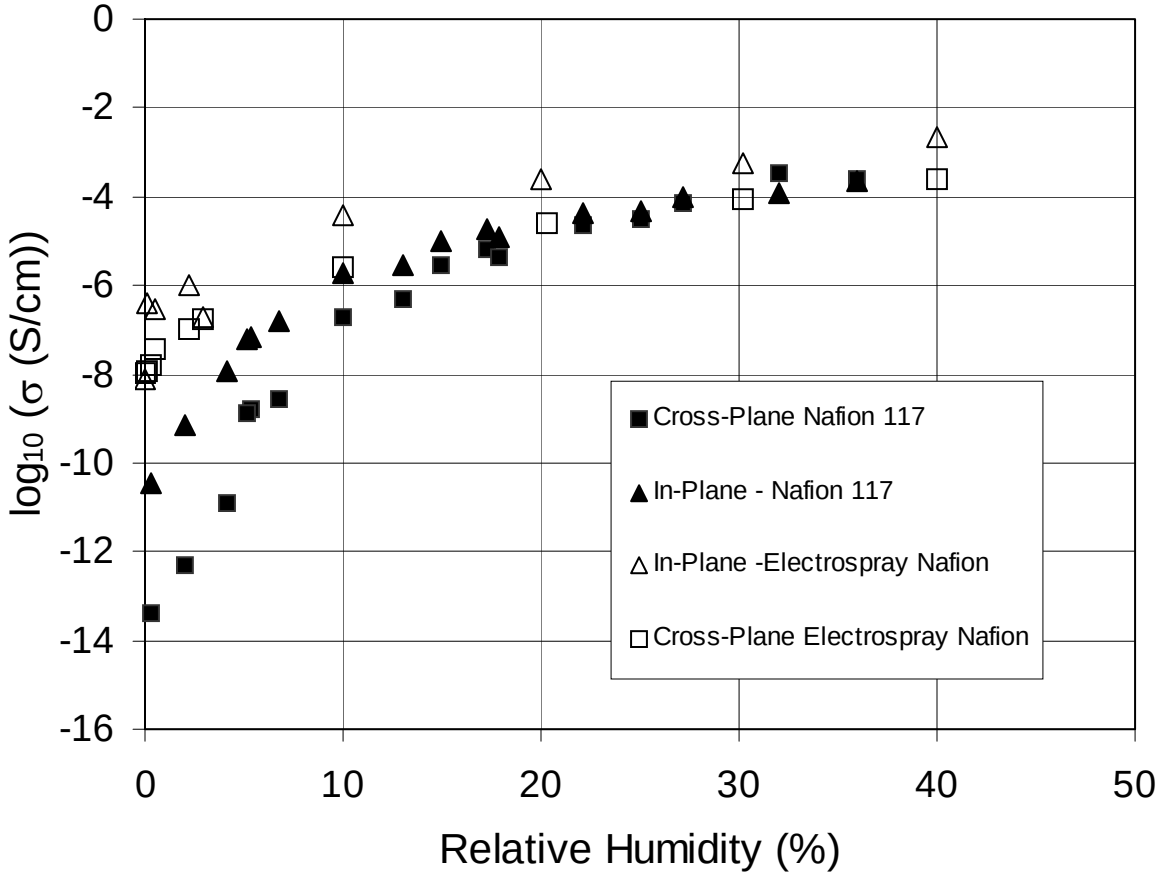

Figure V.F.2 Orientation Effects for Electrosprayed Nafion and Nafion 117

The differences in conductivity for the two orientations of Nafion 117 led to a study of the activation volume differences between the two types of samples. It may be possible that the orientation affects not only the ease with which charge carriers are passed within a sample, but the way in which the protons are transported as well. In order to study these effects, the samples were prepared and tested in a pressure vessel to find their activation volume. Previous studies

have shown the effect of water content on the activation volume for Nafion 117.[20] The data for the in-plane and cross-plane measurements are compared to this previously published data in Figure V.F.3.

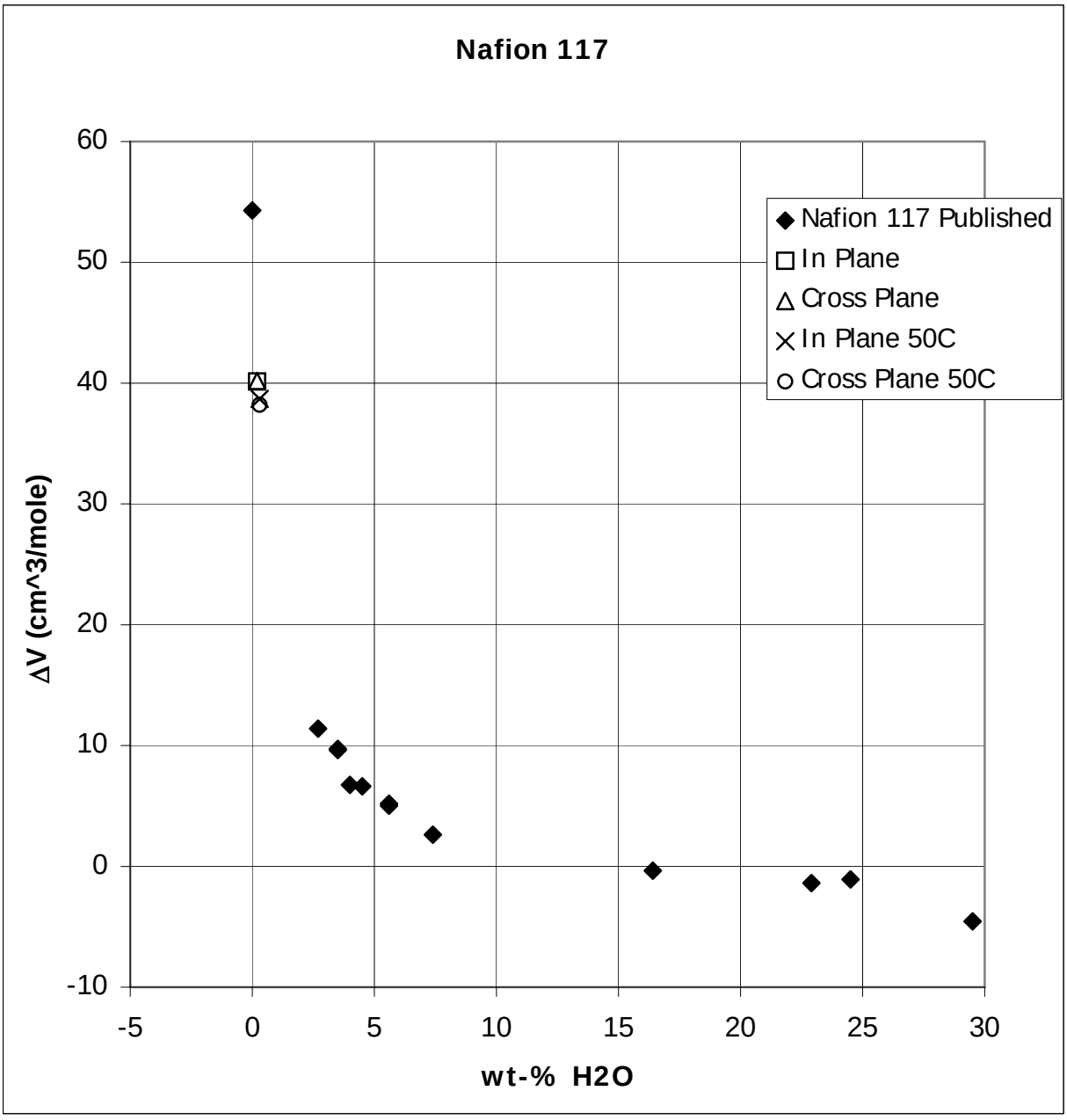

Figure V.F.3 Orientation Effects on Activation Volume for Nafion 117[20]

This data shows four different measurements compared to the previously published data. All measurements were taken in dry conditions, with two taken for each sample orientation. One pair of measurements was taken at room temperature, and the other pair was taken at 50ºC. This is because the data with which these measurements are being compared is a combination of in-plane and cross-plane measurements. When this material was originally being studied, the impedance analysis equipment was limited in its lowest frequency of 10Hz, and was not able to discern impedance arcs for extremely dry in-plane samples. This is because the resistance for these samples is so large. Thus, in order to take a dry measurement, a cross-plane orientation was used. This dry measurement was also taken at an elevated temperature, in order to further enhance the conductance.

The results in Figure V.F.3 are able to confirm that it was acceptable for the researchers to use two different orientations in the original measurements of activation volume for Nafion 117. This is because the orientation volumes for the in-plane and cross-plane orientations do not differ. Thus, the proton conduction mechanisms for the two in dry conditions are the same. Also the use of high temperature does not affect the results significantly, and therefore, this also is an acceptable practice. It can be seen in this figure, that all four new data points correlate with the published data, and fall on the asymptotic line connecting the two driest data points.

VI Conclusion

Electrosprayed Nafion was compared to the commercially available Nafion 117 on the basis of its conductivity, dielectric properties, material swelling, activation volume, diffusion coefficients, and spin lattice relaxation times. The Electrosprayed Nafion was found to have similar water absorption when exposed to the same environmental relative humidity, as well as

similar conductivities for the same water contents. The Electrosprayed Nafion was found to have resonance peaks in the imaginary dielectric constant, which mimic those of the extruded membrane. The activation enthalpy and f_0 coefficient for the gamma relaxation peak of the Electrosprayed Nafion was comparable to the Nafion 117. The Electrosprayed Nafion had activation volumes analogous to those previously published for Nafion 117. Lastly, using Pulse Gradient Spin-Echo NMR, the diffusion coefficients for Electrosprayed Nafion match the extruded; however, the spin lattice relaxation times were significantly lower.

This data supports the use of electrospraying as a deposition technique for use in Nafion based PEM fuel cells. The electrospraying of the samples does not significantly change the conductivity or water transport properties of the membranes. This means that the more cost effective Electrosprayed Nafion is a strong candidate for mass production of fuel cells. The differences in spin lattice relaxation time, and water uptake under wetted conditions are features that need to be addressed as a matter of scientific understanding of the materials, but pose no issues in the use of these materials in practical conditions.

Electrical properties of PEMs are not the only aspect that needs to be addressed before they become viable candidates for use in fuel cells. Electrosprayed Nafion was noticeably fragile in dry environments; thus, some sort of strength or rheological testing must be performed on this material. DMA testing or torsional rheology may be possibilities for continued mechanical experimentation of these materials. The dry strength may be improved by thermal or chemical annealing using methanol or some other similar solvent and warrants further study.

The assumption that Electrosprayed Nafion can mass produce fuel cell MEAs is predicated on the idea that the two electrodes and the membrane can all be electrosprayed together prior to use in fuel cells. These assumptions must be tested, and MEAs that are

produced will have to be tested to ensure that the electrodes don't interfere with the conduction properties. The electrodes may pose other problems as well, such as restriction on water removal. CO poisoning is a crucial concern when studying electrode properties; these studies would also have to ensure that the electrospraying process doesn't impede the catalytic reactions at the electrodes.

The comparisons conducted prior to the observation of orientation effects in Nafion 117 showed Electrosprayed Nafion to be an equal candidate for use in PEM fuel cells on the basis of proton conduction. The orientation data however, suggests that Electrosprayed Nafion is a better candidate than Nafion 117 for use in PEM fuel cells. It shows both higher conductivities in dry environments, as well as no orientation dependent difference. This means that in actual fuel cell usage, a cross-plane orientation, the Electrospray Nafion is more conductive than Nafion 117 be several orders of magnitude. Combined with its less expensive deposition process Electrosprayed Nafion may very well become the new benchmark material for use in PEM fuel cells.

Appendix A: Dynamic Mechanical Analysis

Dynamic Mechanical Analysis[25] (DMA) is a method of using mechanical vibration to evaluate the materials response to mechanical stress. Typically two types of parameters are measured, the loss tangents and moduli. Loss tangents are a measure of how much mechanical vibration energy is transformed into heat, and thus lost to the environment. The loss tangent can be considered to be the damping of the material. The moduli on the other hand are a measure of how energy can be stored in the material in a spring-like manner.

The moduli that result from DMA testing of materials are similar to the familiar Young's modulus, but are fundamentally different in that they are treated as a complex quantity. The real part of the modulus is related to energy storage, and the imaginary part is the loss. The two types of moduli that are found in the dynamic mechanical analysis of a material are the tensile and shear moduli. The loss tangent is found by dividing the imaginary coefficient by the real, Eq A.2.

Tensile Modulus = $E^* = E' + iE''$ Eq A.1

Loss tangent = $\tan(\delta) = \frac{E''}{E'}$ Eq A.2

Young's modulus is the initial slope of the stress-strain curve. This means that it is the change in the strain of the material in relation to an applied stress. The tensile modulus derived from DMA is found from the phase shift between a vibrational stress input and the lagging strain response of the material. Part of the benefit of this data is its usefulness in quantifying the material strength of the sample. The results of a mechanical analysis of the material help classify it as brittle or ductile depending on the relative humidity.

This data is useful because of its relation to the conductivity measurements also being performed on the samples[26]. To visualize the relationship between the mechanical and dielectric aspects of energy dissipation it will once again be helpful to imagine the protons as a series of point charges. As they are conducted through the membrane, the protons undergo a series of collisions. In these collisions part of the protons energy is given off as heat. This lost energy is similar to the heat energy lost when the material undergoes a mechanical vibration.

There are many types of mechanical tests that can quantify the strength of these materials. It may be possible to use static tensile testing, or torsional rheological instrumentation for measuring the change from brittle dry samples to more elastic wet samples. DMA is one of the best candidates for these measurements, because it also provides information on mechanical relaxation. There is a strong correlation between the relaxation peaks in the complex tensile modulus and those observed in the complex dielectric constant. This would enable a better understanding of all the factors at play in proton conduction.

VII References

[1] Office of Naval Research. "Science & Technology – Grand Challenges Signup." www.onr.navy.mil/sci_tech/grandc.htm

[2] Kenawy, E; Layman, J.M.; Watkins, J.R.; Bowlin, G.L.; Matthews, J.A.; Simpson, D.G.; Wnek. *Biomaterials*, **2003**, 24, 907.

[3] Appleby, A.J.; Foulkes, F.R. Fuel Cell Handbook. Krieger, Malabar, Fla. **1993**.

[4] Jones, Richard A.L. Soft Condensed Matter. Oxford University Press, New York, New York. **2002**.

[5] Gersten, Joel I.; Smith, Frederick W. The Physics and Chemistry of Materials. Wiley Interscience Publication, New York, New York. **2001**.

[6] Yeo, S.C.; Eisenberg, A. *Journal of Applied Polymer Science,* **1977**, 21, 875.

[7] Elliot, J.A.; James, P.J.; McMaster, T.J.; Newton, J.M.; Elliot, A.M.S.; Hanna, S.; Miles, M.J. e-Polymers. **2001** 022.

[8] Trevino, S.F.; Young, S.K. 23rd Army Science Conference Poster Session. Poster 21. **2002**.

[9] Wintersgill, M.C.; Fontanella, J.J. *Electrochemica Acta* **1998**, 43, 1533.

[10] Sanders, E.H.; McGrady, K.A.; Wnek, G.E.; Edmondson, C.A.; Mueller, J.M.; Wintersgill, M.C.; Fontanella, J.J. Gustage, S.; Greenbaum, S.G. *Journal of Power Sources*. **2004** 129, 55

[11] Macdonald, J. Ross. Impedance Spectroscopy: Emphasizing Solid Materials and Systems. Wiley Interscience Publication, New York, New York. **1987**.

[12] Zawodzinski, Jr.; T.A.; Derouin, D.; Radzinski, S.; Sherman, R.J.; Smith, V.T.; Springer, T.E.; Gottesfeld, S. *J. Electrochem. Soc.* **1993**, 140, 1041.

[13] Yea, R.S. *J. Electrochem. Soc.* **1983**, 130, 533.

[14] Agmon, N. *Chemical Physics Letters* **1995** 244, 456

[15] Fontanella, J.J.; Edmondson, C.A.; Wintersgill, M.C. *Macromolecules* **1996**, 29, 4944.

[16] Fontanella, J.J.; McLin, M.G.; Wintersgill, M.C. *Journal of Polymer Science* **1994**, 32, 501.

[17] Jonscher, A.K.; Dielectric Relaxation in Solids. Chelsea Dielectrics Press. London. 1983

[18] Daniel, V.V.; Dielectric Relaxation. Academic Press. London. 1967

[19] Suarez, S. Personal Communications.

[20] Stejskal, E.O.; Tanner, J.E. *The Journal of Chemical Physics* **1965** 42, 288.

[21] Antalek, B; *Concepts in Magnetic Resonance* **2002** 12, 4.

[22] Edmondson, C.A.; Fontanella, J.J. *Solid State Ionics* **2002**, 152-153, 355.

[23] Edmondson, C.A.; Fontanella, J.J.; Chung, S.H.; Greenbaum, S.G.; Wnek, G.E. *Electrochimica Acta,* **2001**, 46, 1623.

[24] Suarez, S; Greenbaum, S.G. NMR Investigation of Orientation Dependence of the structure and dynamics in Nafion 117. Manuscript in Preparation.

[25] Menard, Kevin P. Dynamic Mechanical Analysis: A Practical Introduction. CRC Press, Washington, DC. 1999.

[26] Shepard, D.D.; Twombly, B. *Thermochimica Acta,* **1996**, 272, 125.